THEORETICAL MODEL AND COMPUTATIONAL PROCEDURE TO EVALUATE THE NSM FRP STRIPS SHEAR STRENGTH CONTRIBUTION TO A RC BEAM

Vincenzo Bianco [1], Giorgio Monti [2] and J.A.O. Barros [3]

Abstract: This paper presents a closed-form procedure to evaluate the shear strength contribution provided to a Reinforced Concrete (RC) beam by a system of Near Surface Mounted (NSM) Fiber Reinforced Polymer (FRP) strips. This procedure is based on the evaluation of: a) the *constitutive law* of the average-available-bond-length NSM FRP strip effectively crossing the shear crack and b) the *maximum effective capacity* it can attain during the loading process of the strengthened beam. Due to complex phenomena, such as: a) interaction between forces transferred through bond to the surrounding concrete and the concrete fracture, and b) interaction among adjacent strips, the NSM FRP strip constitutive law is largely different than the linear elastic one characterizing the FRP behavior in tension. Once the constitutive law of the average-available-bond-length NSM strip is reliably known, its maximum effective capacity can be determined by imposing a coherent *kinematic mechanism*. The self-contained and ready-to-implement set of analytical equations and logical operations is presented along with the main underlying physical-mechanical principles and assumptions. The formulation proposed is appraised against some of the most recent experimental results, and its predictions are also compared with those obtained by a recently developed more sophisticated model.

Keywords: FRP; NSM; Computational Procedure; Shear Strengthening; Concrete Fracture; Debonding; Tensile Rupture.

Introduction

Shear strengthening of RC beams by NSM technique consists of gluing FRP strips by a powerful structural adhesive into thin shallow slits cut onto the concrete cover of the beam web lateral faces. A comprehensive three-dimensional mechanical model to predict the NSM FRP strips shear strength contribution to a RC beam was recently developed (Bianco 2008, Bianco *et al.* 2009a-b and 2010). Despite its consistency with experimental recordings, that model turned out to be somehow cumbersome to be easily implemented and accepted by professional structural engineers. The aim of the present work is to develop a simpler computational

[1] Post Doctoral Student, Dept. of Structural Engrg. and Geotechnics, Sapienza University of Rome, via A. Gramsci 53, 00197 Rome, Italy. E-mail: vincenzo.bianco@uniroma1.it, corresponding Author. Tel. +39 0649919254, Fax. +39 063221449.
[2] Full Professor, Dept. of Structural Engrg. and Geotechnics, Sapienza University of Rome, via A. Gramsci 53, 00197 Rome, Italy. E-mail: giorgio.monti@uniroma1.it.
[3] Associate Professor, Dept. of Civil Engineering, University of Minho, Campus de Azurém, 4810-058 Guimarães, Portugal. E-mail: barros@civil.uminho.pt.

procedure that has to be: a) *mechanically-based* and b) *simple to implement*. As to the first point, it has to fulfill equilibrium, kinematic compatibility and constitutive laws. As to the second point, it has to be a design tool that is easy to apply. For this purpose, a reasonable compromise between accuracy of prediction and computational demand has to be achieved. Excessively simplified assumptions, which would provide too roughly conservative estimates of the shear strength contribution provided by a system of NSM FRPs, should be avoided since they could lead to uneconomical design solutions, discouraging application, further improvement and spreading of the technique. A relatively simple model can be derived from the more sophisticated one by introducing the following simplifications (Bianco 2008): 1) a bi-linear rigid-softening local bond stress-slip diagram is adopted instead of a multilinear diagram, 2) concrete fracture surface is assumed as semi-pyramidal instead of semi-conical, 3) attention is focused on the average-available-bond-length NSM FRP strip glued on the relevant prism of surrounding concrete, 4) determining the constitutive law of the average-available-bond-length NSM strip, along the approach followed for Externally Bonded Reinforcement (EBR) by Monti *et al.* (2003), and 5) determining the maximum effective capacity attainable by the average-available-bond-length NSM strip placed along the CDC, imposing a coherent kinematic mechanism (*e.g.* Monti *et al.* 2004, Monti and Liotta 2007). The main features of the resulting modeling strategy are reported hereafter.

During the loading process of a RC beam subject to shear, when concrete average tensile strength f_{ctm} is attained at the web intrados (Fig. 1), some shear cracks originate therein and successively progress towards the web extrados. Those cracks can be thought as a single Critical Diagonal Crack (CDC) inclined of an angle θ with respect to the beam longitudinal axis (Fig. 1a). The CDC can be schematized as an inclined plane dividing the web into two portions sewn together by the crossing strips (Fig. 1a). At load step t_1, the two web parts, separated by the CDC, start moving apart by pivoting around the crack end whose trace, on the web face, is point *E* in Fig. 1a. From that step on, by increasing the applied load, the CDC opening angle $\gamma(t_n)$ progressively widens (Fig. 1a). The strips crossing the CDC oppose its widening by anchoring to the surrounding concrete to which they transfer, by bond, the force originating at their intersection with the CDC, O_i^l, as a result of the imposed end slip $\delta_{Li}[\gamma(t_n)]$. The capacity of each strip is provided by its available bond length L_{fi} that is the shorter between the two parts into which the crack divides its actual length L_f (Fig. 1a). Bond is the mechanism through which stresses are transferred to the surrounding concrete (Yuan *et al.* 2004, Mohammed Ali *et al.* 2006 and 2007, Bianco *et al.* 2007). The local bond stress-slip relationship $\tau(\delta)$, comprehensively simulating the mechanical phenomena occurring at 1) the strip-adhesive interface, 2) within the adhesive layer and at 3) the

adhesive-concrete interface, can be represented, in a simplified way, by a bi-linear curve (Fig. 1b). The subsequent phases undergone by bond during the loading process, representing the physical phenomena occurring in sequence within the adhesive layer by increasing the imposed end slip, are: "rigid", "softening friction" and "free slipping" (Fig. 1b) (Bianco 2008). The first *rigid* branch (0-τ_0) represents the overall initial shear strength of the joint, independent of the deformability of the adhesive layer and attributable to the micro-mechanical and mainly chemical properties of the involved materials and relative interfaces. In fact, the parameter τ_0 is the average of the following physical entities encountered in sequence by stresses flowing from the strip to the surrounding concrete, *i.e.*: adhesion at the strip-adhesive interface, cohesion within the adhesive itself, and adhesion at the adhesive-concrete interface (*e.g.* Sekulic and Curnier 2006, Zhai *et al.* 2008).

The $\tau(\delta)$ curve adopted (Fig. 1b) envisages that, by imposing increasing end slips to the FRP strip, cracks form instantaneously within the adhesive layer, both orthogonally to the (inclined) tension isostatics and along the strip-adhesive and adhesive-concrete interfaces (*e.g.* Sena-Cruz and Barros 2004). Stresses are transferred by friction and micro-mechanical interlock along those micro-cracks. Nonetheless, by imposing increasing end slips, those cracks progressively become smoother (*softening friction* phase) up to the point ($\delta_{Li} = \delta_1$) in which friction can no longer be mobilized and the strip is pulled out without having to overcome any restraint left (*free slipping* phase).

The constitutive law $V_{fi}\left(L_{Rfi};\delta_{Li}\right)$ of an NSM FRP strip, *i.e.* the force transmissible by a strip with resisting bond length L_{Rfi} as function of the imposed end slip δ_{Li}, can be determined by analyzing the behavior of the simple structural element composed of the NSM FRP strip within a concrete prism (Fig. 1a,c-d) whose transversal dimensions are limited by the spacing s_f between adjacent strips and half of the web cross section width $b_w/2$. In this way, the problem of interaction between adjacent strips (Dias and Barros 2008, Rizzo and De Lorenzis 2009) is taken into account in a simplified way, *i.e.*, by limiting the concrete volume into which subsequent fractures can form, to the amount of surrounding concrete pertaining to the single strip in dependence of s_f and b_w. Moreover, even though here neglected, the interaction with existing stirrups may be also accounted for by limiting the transversal dimension of the concrete prism to a certain ratio of $b_w/2$, since the larger the amount of stirrups, the shallower concrete fracture is expected to be (Bianco *et. al* 2006) even if, in this respect, further research is necessary.

In particular, in the present work, attention is focused on the system composed of the strip with the average value of available bond length glued on the pertaining prism of surrounding concrete (Fig. 1c-d).

The failure modes of an NSM FRP strip subject to an imposed end slip comprise, depending on the relative mechanical and geometrical properties of the materials involved: debonding, tensile rupture of the strip, concrete semi-pyramidal tensile fracture and a mixed shallow-semi-pyramid-plus-debonding failure mode (Fig. 1e). The term *debonding* is adopted to designate loss of bond due to damage initiation and propagation within the adhesive layer and at the FRP strip-adhesive and adhesive-concrete interfaces, so that the strip pulling out results (Fig. 1e). When principal tensile stresses transferred to the surrounding concrete attain its tensile strength, concrete fractures along a surface, envelope of the compression isostatics, whose shape can be conveniently assumed as a semi-pyramid with principal generatrices inclined of an angle α with respect to the strip longitudinal axis (Fig. 1c-d). Increasing the imposed end slip can result in subsequent semi-pyramidal and coaxial fracture surfaces in the concrete surrounding the NSM strip. These progressively reduce the resisting bond length L_{Rfi} that is the portion of the initial available bond length L_{fi} still bonded to concrete. Those subsequent fractures can either progress up to the free end, resulting in a *concrete semi-pyramidal failure*, or stop progressing midway between loaded and free end, resulting in a *mixed-shallow-semi-pyramid-plus-debonding* failure (Fig. 1e). Moreover, regardless of an initial concrete fracture, the strip can *rupture* (Fig. 1e).

The formulation obtained by this strategy is presented in the following sections along with the main mechanical bases.

Calculation procedure

The input parameters include (Fig. 2): beam cross-section web's depth h_w and width b_w; inclination angle of both CDC and strips with respect to the beam longitudinal axis, θ and β, respectively; strips spacing measured along the beam axis s_f; angle α between axis and principal generatrices of the semi-pyramidal fracture surface (Fig. 1c-d); concrete average compressive strength f_{cm}; strips tensile strength f_{fu} and Young's modulus E_f; thickness a_f and width b_f of the strip cross-section; increment $\dot{\delta}_{Li}$ of the imposed end slip; values of bond stress τ_0 and slip δ_1 defining the adopted local bond stress-slip relationship (Fig. 1b):

$$\tau(\delta)=\begin{cases}\tau_0\left(1-\dfrac{\delta}{\delta_1}\right) & 0<\delta\le\delta_1\\ 0 & \delta>\delta_1\end{cases} \tag{1}$$

The geometrical configuration is adopted in which the minimum integer number $N^l_{f,\mathrm{int}}$ of strips cross the CDC with the first one placed at a distance equal to s_f from the crack origin (Fig. 1a). This configuration corresponds

to the minimum of the sum of all the available bond lengths L_{fi}. $N^{l}_{f,\text{int}}$ is obtained by rounding off the real number to the lowest integer, as follows:

$$N^{l}_{f,\text{int}} = \text{round off}\left[h_w \cdot \frac{(\cot\theta + \cot\beta)}{s_f} \right] \tag{2}$$

and the average available bond length $\overline{L}_{fi}$ is obtained by:

$$\overline{L}_{fi} = \frac{1}{N^{l}_{f,\text{int}}} \cdot \sum_{i=1}^{N^{l}_{f,\text{int}}} L_{fi} \tag{3}$$

with:

$$L_{fi} = \begin{cases} i \cdot s_f \cdot \dfrac{\sin\theta}{\sin(\theta+\beta)} & \text{for} \quad x_{fi} < \dfrac{h_w}{2} \cdot (\cot\theta + \cot\beta) \\ L_f - i \cdot s_f \cdot \dfrac{\sin\theta}{\sin(\theta+\beta)} & \text{for} \quad x_{fi} \geq \dfrac{h_w}{2} \cdot (\cot\theta + \cot\beta) \end{cases} \tag{4}$$

and:

$$x_{fi} = i \cdot s_f \tag{5}$$

After having defined the geometrical characteristics of the simple structural system composed of the average-available-bond-length strip within the relevant prism of surrounding concrete, it is necessary to determine its constitutive law $V_{fi}\left(\overline{L}_{fi}; \delta_{Li}\right)$ and the corresponding maximum effective capacity $V_{fi}^{\max}$, as explained hereafter. Once $V_{fi}^{\max}$ has been obtained, the actual V_f and design V_{fd} values of the NSM shear strength contribution can be obtained by Eq. (36).

Constitutive law of a single NSM FRP strip

The mechanical behaviour of an FRP strip glued near the surface of a concrete prism and subjected to an increasing imposed end slip is very complex. That complexity is due to the interaction between the mechanism of force transfer to the surrounding concrete through bond stresses, mobilized along the glued surface, and the possibility of concrete fracture. Due to this interaction, the simple structural system composed of a single strip, the adhesive and the surrounding concrete, undergoes changes during the loading process since, each time concrete fractures, the resisting bond length reduces accordingly. In particular, the different features assumed by that system throughout the loading process are function not only of the load step t_n, but also of the iteration q_m in correspondence of t_n (Bianco 2008). In fact, for each t_n, that system undergoes modifications up to reaching the equilibrium configuration q_e. Whenever concrete fractures, the mechanism of force transfer to the

surrounding concrete leaps forward towards the strip's free end. In general, in correspondence of each leap, the overall transfer length $L_{tr,fi}\left(L_{Rfi};\delta_{Li}\right)$ increases and the resisting bond length decreases (Fig. 1c-d). Thus, in general, at each leap, concrete tensile fracture capacity increases and at the same time the bond-transferred force decreases, until equilibrium is attained. In this scenario, in order to determine the comprehensive constitutive law $V_{fi}\left(\overline{L}_{fi};\delta_{Li}\right)$ of the average-available-bond-length NSM FRP strip bonded to the relevant prism of surrounding concrete, it is necessary to carry out an incremental procedure that simulates the imposed end slip $\delta_{Li}(t_n)$ and to check, at each t_n, either if concrete is capable of carrying the bond-transferred stresses without undergoing fracture, or if a concrete fracture occurs and the system has to be modified accordingly.

Bond-based constitutive law

The bond behaviour of an NSM FRP strip subject to an increasing imposed end slip can be modelled by fulfilling equilibrium, kinematic compatibility and constitutive laws of both adhered materials (concrete and FRP) and local bond between themselves (Bianco 2008). In this way, it is possible to obtain closed-form analytical equations for both the bond-based constitutive law $V_{fi}^{bd}\left(L_{Rfi};\delta_{Li}\right)$ of a single strip and the corresponding bond transfer length $L_{tr,fi}^{bd}\left(L_{Rfi};\delta_{Li}\right)$. The latter two quantities represent: the force a strip of resisting bond length L_{Rfi} can transfer by bond, as function of δ_{Li}, and the corresponding amount of L_{Rfi} along which bond is mobilized, respectively. Once the invariant distribution of shear stress $\tau(x)$ and slip $\delta(x)$ is determined for an infinite value of L_{Rfi} (Fig. 3a), $L_{tr,fi}^{bd}$ and V_{fi}^{bd} can be determined for any finite value of L_{Rfi} (Fig. 3b-g) considering the migration of $\tau(x)$ along L_{Rfi}, from the loaded end (LE) to the free end (FE), by increasing δ_{Li}. The analytical equations of $L_{tr,fi}^{bd}\left(L_{Rfi};\delta_{Li}\right)$ and $V_{fi}^{bd}\left(L_{Rfi};\delta_{Li}\right)$, presented below and plotted in Fig. 4, can be determined by: a) considering the relative position of L_{Rfi} with respect to the invariant distribution of $\tau(x)$ and $\delta(x)$, and b) integrating $\tau(x)$, respectively (Bianco 2008, Bianco *et. al* 2009b). Those analytical equations envisage (Figs. 3-4), for a given L_{Rfi}, three phases, whose limits ($\delta_{L1};\delta_{L2};\delta_{L3}$) are function of the value assumed by L_{Rfi} with respect to the effective bond length L_{tr1} that is the value of resisting bond length beyond which any further increase of length does not produce any further increase of the maximum force transmissible by bond. In the first phase (Figs. 4,3b), the force transmitted by bond stresses increases up to reaching the peak in correspondence of

$\delta_{L1}(L_{Rfi})$ that is (Fig. 3c), for $L_{Rfi} < L_{tr1}$, the δ_{Li} for which the invariant distribution of bond stresses has reached the strip's free end while, for $L_{Rfi} \geq L_{tr1}$, the δ_{Li} for which $L^{bd}_{tr,fi} = L_{tr1}$. The second phase (Figs. 4,3d), for $L_{Rfi} < L_{tr1}$, is characterized by a decrease of V^{bd}_{fi} and a constancy of $L^{bd}_{tr,fi}$ while, for $L_{Rfi} \geq L_{tr1}$, V^{bd}_{fi} remains constant and equal to the peak V^{bd}_1 and $L^{bd}_{tr,fi}$ goes on increasing up to $\delta_{L2}(L_{Rfi})$. $\delta_{L2}(L_{Rfi})$ is (Figs. 4,3e), for $L_{Rfi} < L_{tr1}$, the δ_{Li} for which the null value of the invariant distribution of $\tau(x)$ has reached the loaded end while, for $L_{Rfi} \geq L_{tr1}$, the δ_{Li} for which the value τ_0 of the invariant distribution of $\tau(x)$ has reached the free end. In the third phase (Figs. 4,3f), the invariant distribution of bond stresses progressively moves away from L_{Rfi}, regardless of its value, resulting in a decrease of V^{bd}_{fi} up to zero and in a constant value of $L^{bd}_{tr,fi}$ that is equal to L_{Rfi}. $\delta_{L3}(L_{Rfi})$ is (Figs. 4,3g), for each L_{Rfi}/L_{tr1}, the δ_{Li} in correspondence of which the null value of the invariant distribution of $\tau(x)$ has reached the free end. Note that, for continuity, for $L_{Rfi} = L_{tr1}$ it is $\delta_{L1}(L_{tr1}) = \delta_{L2}(L_{tr1}) \equiv \delta_1$ and the second phase reduces to a point (Fig. 4).

The bond transfer length is as follows:

$$
\begin{cases}
L^{bd}_{tr,fi}(L_{Rfi};\delta_{Li}) = L^{sf}_{tr}(\delta_{Li}) = \dfrac{1}{\lambda}\cdot\arccos\left(1-\dfrac{\lambda^2}{\tau_0\cdot J_1}\cdot\delta_{Li}\right) & 0.0 \leq \delta_{Li} \leq \delta_{L1}(L_{Rfi}) \\
\begin{cases} L^{bd}_{tr,fi}(L_{Rfi} < L_{tr1};\delta_{Li}) = L_{Rfi} \\ L^{bd}_{tr,fi}(L_{Rfi} \geq L_{tr1};\delta_{Li}) = L_{tr1} + L^{fs}_{tr}(\delta_{Li}) \end{cases} & \delta_{L1}(L_{Rfi}) < \delta_{Li} \leq \delta_{L2}(L_{Rfi}) \\
L^{bd}_{tr,fi}(L_{Rfi};\delta_{Li}) = L_{Rfi} & \delta_{L2}(L_{Rfi}) < \delta_{Li} \leq \delta_{L3}(L_{Rfi}) \\
L^{bd}_{tr,fi}(L_{Rfi};\delta_{Li}) = 0.0 & \delta_{Li} > \delta_{L3}(L_{Rfi})
\end{cases}
\tag{6}
$$

and the bond-based constitutive law:

$$
\begin{cases}
V^{bd}_{fi}(L_{Rfi};\delta_{Li}) = L_p\cdot J_3\cdot\lambda\cdot\left\{C^{sf}_1\cdot\left[\cos\left(\lambda\cdot L^{sf}_{tr}(\delta_{Li})\right)-1\right]-C^{sf}_2\cdot\sin\left(\lambda\cdot L^{sf}_{tr}(\delta_{Li})\right)\right\} & 0.0 \leq \delta_{Li} \leq \delta_{L1}(L_{Rfi}) \\
\begin{cases} V^{bd}_{fi}(L_{Rfi} < L_{tr1};\delta_{Li}) = L_p\cdot J_3\cdot\lambda\cdot\left[C^{sf}_1\cdot\cos\left(\lambda\cdot x^{sf}\right)-C^{sf}_2\cdot\sin\left(\lambda\cdot x^{sf}\right)\right]_{L^{sf}_{tr}(\delta_{Li})-L_{Rfi}}^{L^{sf}_{tr}(\delta_{Li})} \\ V^{bd}_{fi}(L_{Rfi} \geq L_{tr1};\delta_{Li}) = V^{bd}_{f1} \end{cases} & \delta_{L1}(L_{Rfi}) < \delta_{Li} \leq \delta_{L2}(L_{Rfi}) \\
V^{bd}_{fi}(L_{Rfi};\delta_{Li}) = L_p\cdot J_3\cdot\lambda\cdot\left[C^{sf}_1\cdot\cos\left(\lambda\cdot x^{sf}\right)-C^{sf}_2\cdot\sin\left(\lambda\cdot x^{sf}\right)\right]_{L_{tr1}+L^{fs}_{tr}(\delta_{Li})-L_{Rfi}}^{L_{tr1}} & \delta_{L2}(L_{Rfi}) < \delta_{Li} \leq \delta_{L3}(L_{Rfi}) \\
V^{bd}_{fi}(L_{Rfi};\delta_{Li}) = 0.0 & \delta_{Li} > \delta_{L3}(L_{Rfi})
\end{cases}
\tag{7}
$$

where:

$$L_p = 2 \cdot b_f + a_f \tag{8}$$

is the effective perimeter of the strip cross-section, and:

$$\frac{1}{\lambda^2} = \frac{\delta_1}{\tau_0 \cdot J_1}; J_1 = \frac{L_p}{A_f} \cdot \left[\frac{1}{E_f} + \frac{A_f}{A_c \cdot E_c} \right]; J_2 = \frac{E_f \cdot E_c \cdot A_c}{E_c \cdot A_c + E_f \cdot A_f}$$
$$J_3 = \frac{E_f \cdot A_f \cdot E_c \cdot A_c}{L_p \cdot \left(A_c \cdot E_c + A_f \cdot E_f \right)}; C_1^{sf} = \delta_1 - \frac{\tau_0 \cdot J_1}{\lambda^2}; C_2^{sf} = -\frac{\tau_0 \cdot J_1}{\lambda^2} \tag{9}$$

are bond-modeling constants (Bianco 2008, Bianco *et al.* 2009b), with $A_p = a_f \cdot b_f$ and $A_c = s_f \cdot b_w / 2$ the cross-section of the strip and the concrete prism, respectively.

Moreover, the effective bond length L_{tr1} and the corresponding maximum bond force V_{f1}^{bd} are given by:

$$L_{tr1} = \frac{\pi}{2 \cdot \lambda}; V_{f1}^{bd} = L_p \cdot J_3 \cdot \lambda \cdot \left[\frac{2 \cdot \tau_0 \cdot J_1}{\lambda^2} - \delta_1 \right] \tag{10}$$

The value of resisting bond length undergoing softening friction, as function of the imposed end slip, is given by:

$$L_{tr}^{sf}(\delta_{Li}) = \frac{1}{\lambda} \cdot \arccos\left[1 - \frac{\lambda^2}{\tau_0 \cdot J_1} \cdot \delta_{Li} \right] \tag{11}$$

and the value of resisting bond length undergoing free slipping:

$$L_{tr}^{fs}(\delta_{Li}) = \frac{A_f \cdot J_2 \cdot (\delta_{Li} - \delta_1)}{V_{f1}^{bd}} \tag{12}$$

The resisting bond length-dependent values of imposed end slip defining the extremities of the three bond phases, are given by (Fig. 3b-g):

$$\delta_{L1}\left(L_{Rfi}\right) = \begin{cases} C_1^{sf} \cdot \sin\left(\lambda \cdot L_{Rfi}\right) + C_2^{sf} \cdot \cos\left(\lambda \cdot L_{Rfi}\right) + \dfrac{\tau_0 \cdot J_1}{\lambda^2} & \text{for } L_{Rfi} < L_{tr1} \\ \delta_1 & \text{for } L_{Rfi} \geq L_{tr1} \end{cases} \tag{13}$$

$$\delta_{L2}\left(L_{Rfi}\right) = \begin{cases} \delta_1 & \text{for } L_{Rfi} < L_{tr1} \\ \delta_1 + \dfrac{V_{f1}^{bd}}{A_f \cdot J_2} \cdot \left(L_{Rfi} - L_{tr1}\right) & \text{for } L_{Rfi} \geq L_{tr1} \end{cases} \tag{14}$$

$$\delta_{L3}\left(L_{Rfi}\right) = \delta_1 + \frac{L_{Rfi} \cdot V_{f1}^{bd}}{A_f \cdot J_2} \tag{15}$$

Concrete tensile fracture capacity

The concrete tensile fracture capacity $V_{fi}^{cf}\left(L_{tr,fi}\right)$ is obtained by spreading the concrete average tensile strength f_{ctm} over the semi-pyramidal surface (Fig. 1c-d) of height equal to the total transfer length $L_{tr,fi}$, orthogonally to it in each point. By integrating one obtains:

$$V_{fi}^{cf}\left(L_{tr,fi}\right) = f_{ctm}\cdot\min\left\{L_{tr,fi}\cdot\tan\alpha;\frac{b_w}{2}\right\}\cdot\sin\left(\theta+\beta\right)\cdot \\ \cdot\left(\min\left\{\frac{s_f\cdot\sin\beta}{2\cdot\sin\left(\theta+\beta\right)};\frac{L_{tr,fi}\cdot\sin\alpha}{\sin\left(\theta+\beta+\alpha\right)}\right\}+\min\left\{\frac{s_f\cdot\sin\beta}{2\cdot\sin\left(\theta+\beta\right)};\frac{L_{tr,fi}\cdot\sin\alpha}{\sin\left(\theta+\beta-\alpha\right)}\right\}\right) \tag{16}$$

where f_{ctm} can be determined from the average compressive strength. The total transfer length is evaluated as reported in next Eq. (17).

Comprehensive constitutive law

At the t_n load step, an iterative procedure ($q_m : q_1 \to q_e$) is carried out in order to determine the equilibrium condition (q_e) in the surrounding concrete depending on the current value of both imposed end slip $\delta_{Li}(t_n)$ and resisting bond length $L_{Rfi}(t_n;q_m)$ (Figs. 5-7). In particular, at the q_m iteration of the t_n load step, based on $L_{Rfi}(t_n;q_m)$ and $\delta_{Li}(t_n)$, the bond transfer length $L_{tr,fi}^{bd}\left[L_{Rfi}(t_n;q_m);\delta_{Li}(t_n)\right]$ and the corresponding bond-transferred force $V_{fi}^{bd}\left[L_{Rfi}(t_n;q_m);\delta_{Li}(t_n)\right]$ are evaluated as reported in Eq. (6) and Eq. (7), respectively. Then, the current value of the total transfer length is evaluated as follows:

$$L_{tr,fi}(t_n;q_m) = L_{fi}^{c}(t_{n-1};q_e) + L_{tr,fi}^{bd}\left[L_{Rfi}(t_n;q_m);\delta_{Li}(t_n)\right] + \Delta L_{fi}^{c}(t_n;q_m) \tag{17}$$

where $L_{fi}^{c}(t_{n-1};q_e)$ is the cumulative depth of the concrete fracture surface resulting from the equilibrium of the preceding t_{n-1} load step and $\Delta L_{fi}^{c}(t_n;q_m)$ is the increment of concrete fracture depth corresponding to the current t_n, accumulated up to the current q_m (Fig. 6c):

$$\Delta L_{fi}^{c}(t_n;q_m) = \sum_{q_1}^{q_{m-1}} L_{tr,fi}^{bd}\left[L_{Rfi}(t_n;q_m);\delta_{Li}(t_n)\right] \tag{18}$$

Then, after having evaluated the concrete fracture capacity $V_{fi}^{cf}\left(L_{tr,fi}\right)$ as indicated in Eq. (16), if it is:

$$V_{fi}^{bd}\left[L_{Rfi}(t_n;q_m);\delta_{Li}(t_n)\right] \geq V_{fi}^{cf}\left[L_{tr,fi}(t_n;q_m)\right] \tag{19}$$

meaning that the surrounding concrete is not capable to carry the bond-transferred force, then it fractures and the bond transfer mechanism leaps forwards towards the free end. Thus, the parameters $L_{Rfi}(t_n;q_{m+1})$ and

$\Delta L^c_{fi}(t_n;q_{m+1})$ are updated ($L_{Rfi}(t_n;q_{m+1})=L_{Rfi}(t_n;q_m)-L^{bd}_{tr,\,fi}\left[L_{Rfi}(t_n;q_m);\delta_{Li}(t_n)\right]$, $\Delta L^c_{fi}(t_n;q_{m+1})=\Delta L^c_{fi}(t_n;q_m)+L^{bd}_{tr,\,fi}\left[L_{Rfi}(t_n;q_m);\delta_{Li}(t_n)\right]$) and iteration is performed (q_{m+1}) (Fig. 5). At each of those leaps, the point representative of the strip state moves from one bond-based constitutive law $V^{bd}_{fi}\left[L_{Rfi}(t_n;q_m);\delta_{Li}\right]$ to the other $V^{bd}_{fi}\left[L_{Rfi}(t_n;q_{m+1});\delta_{Li}\right]$ and, as long as the updated value of L_{Rfi} is larger or equal to the necessary bond transfer length $L^{bd}_{tr}[\delta_{Li}(t_n)]$, such leap is only visible in a three dimensional representation (Fig. 6d). The necessary bond transfer length $L^{bd}_{tr}[\delta_{Li}(t_n)]$ is the bond transfer length that would be necessary, if L_{Rfi} were infinite, to transmit the corresponding force to the surrounding concrete, with $L^{bd}_{tr}[\delta_{Li}(t_n)]=L^{sf}_{tr}[\delta_{Li}(t_n)]$ for $\delta_{Li}(t_n)\le\delta_1$ and $L^{bd}_{tr}[\delta_{Li}(t_n)]=L_{tr1}+L^{fs}_{tr}[\delta_{Li}(t_n)]$ for $\delta_{Li}(t_n)>\delta_1$ (Fig. 3). Note also that, at each q_m iteration, the equality $L_{Rfi}(t_n;q_m)+L^c_{fi}(t_{n-1};q_e)+\Delta L^c_{fi}(t_n;q_m)=L_{Rfi}(t_1;q_1)=\overline{L}_{fi}$ has to be fulfilled (Fig. 6c and Fig. 7c).

More in detail, at the q_m iteration of the t_n load step, if concrete is not in equilibrium ($c_e=0$), one of the following alternatives might occur:

- concrete fracture is deep ($d_f=1$) but it does not reach the free end, *i.e.* the updated resisting bond length $L_{Rfi}(t_n;q_{m+1})$ is not long enough to mobilize, for the current $\delta_{Li}(t_n)$, a bond transfer length as large as the necessary one: $L_{Rfi}<L^{bd}_{tr}[\delta_{Li}(t_n)]$ (Fig. 5). Note that in this case, the passage of the point representative of the strip state from one bond-based constitutive law to the other is also visible in a bi-dimensional representation (Fig. 7);
- concrete fracture is deep ($d_f=1$) and it reaches the free end, *i.e.* the updated resisting bond length $L_{Rfi}(t_n;q_{m+1})$ is null. Note is taken of the current value of the imposed end slip ($\delta_{Lu}\leftarrow\delta_{Li}(t_n)$) and the incremental procedure is terminated since a decision about the comprehensive constitutive law can already be taken ($u=1$) (Fig. 8a).

On the contrary, if at the q_m iteration of the t_n load step, concrete is in equilibrium ($c_e=1$), it is not necessary to iterate and one of the following alternatives might occur:

- the current value of bond-transferred force is larger or equal to the strip tensile rupture capacity ($V^{bd}_{fi}\ge V^{tr}_f$). The incremental procedure is terminated since, even if the surrounding concrete is in

equilibrium, the strip has ruptured ($u = 2$) and note is taken of the ultimate imposed end slip ($\delta_{Lu} \leftarrow \delta_{Li}(t_n)$);

- the next value of the imposed end slip $\delta_{Li}(t_{n+1})$ is larger or equal to the one in correspondence of which the peak bond force is attained for the current value of the resisting bond length $\delta_{Li}(t_{n+1}) \geq \delta_{L1}\left[L_{Rfi}(t_n; q_e)\right]$. Since V_{fi}^{bd} starts to decrease for $\delta_{Li}(t_{n+1})$ (Figs. 6-7), the incremental procedure is terminated and note is taken of the current value of the resisting bond length ($L_{Rfu} \leftarrow L_{Rfi}$) and of its relationship with the effective bond length L_{tr1} ($u \leftarrow 3$ if $L_{Rfu} < L_{tr1}$, $u \leftarrow 4$ if $L_{Rfu} = L_{tr1}$ or $u \leftarrow 5$ if $L_{Rfu} > L_{tr1}$);
- concrete fracture is deep ($d_f = 1$) and it does not reach the free extremity. The incremental procedure is terminated ($u = 6$) (Fig. 8d);
- the next value of the imposed end slip $\delta_{Li}(t_{n+1})$ is smaller than the one where the peak bond force is attained for the current value of the resisting bond length $\delta_{Li}(t_{n+1}) < \delta_{L1}\left[L_{Rfi}(t_n; q_e)\right]$. Then, the imposed end slip is incremented and the iteration carried out.

The incremental procedure described above is terminated and, depending on the phenomenon characterizing the specific case at hand and the type of constitutive law associated (u), the parameters necessary to define $V_{fi}\left(\bar{L}_{fi}; \delta_{Li}\right)$ are returned, *i.e.*:

- deep concrete fracture that reaches the strip's free extremity ($u = 1$) or tensile rupture of the strip ($u = 2$). The parameter necessary to determine the constitutive law is the imposed end slip δ_{Lu} in correspondence of which the peak of $V_{fi}\left(\bar{L}_{fi}; \delta_{Li}\right)$ occurs. $V_{fi}\left(\bar{L}_{fi}; \delta_{Li}\right)$ is given by the first bond phase of Eq. (7) for $0.0 \leq \delta_{Li} \leq \delta_{Lu}$ (Fig. 8a);
- shallow or absent concrete fracture with an ultimate value of resisting bond length smaller ($u = 3$), equal ($u = 4$) or larger ($u = 5$) than the effective bond length. The parameter necessary to determine the comprehensive constitutive law is the ultimate value assumed by the resisting bond length L_{Rfu}. $V_{fi}\left(\bar{L}_{fi}; \delta_{Li}\right)$ is given by Eq. (7) for $L_{Rfi} = L_{Rfu}$ (Fig. 8b-c);
- deep tensile fracture with an ultimate value of resisting bond length very short but not null ($u = 6$). The parameters necessary to determine the comprehensive constitutive law are both the imposed end slip

δ_{Lu} in correspondence of which the peak of $V_{fi}\left(\bar{L}_{fi};\delta_{Li}\right)$ occurs and the ultimate value assumed by the resisting bond length L_{Rfu}. $V_{fi}\left(\bar{L}_{fi};\delta_{Li}\right)$ is given by: the first bond phase of Eq. (7) for $0.0 \le \delta_{Li} \le \delta_{Lu}$, the second bond phase of Eq. (7) for $\delta_{Lu} < \delta_{Li} \le \delta_{L2}\left(L_{Rfu}\right)$ and the third bond phase of Eq. (7) for $\delta_{L2}\left(L_{Rfu}\right) < \delta_{Li} \le \delta_{L3}\left(L_{Rfu}\right)$ (Fig. 8d).

Maximum effective capacity of a single NSM FRP strip

The effective capacity $V_{fi,eff}(\gamma)$ is the average of the NSM FRP strip capacity along the CDC $V_{fi,CDC}(\gamma;\xi)$ for a given value of the CDC opening angle γ (Figs. 9-13), where ξ is the reference system assumed along the CDC (Fig. 1a). $V_{fi,CDC}(\gamma;\xi)$ is obtained by introducing the kinematic compatibility ($\delta_{Li}(\gamma;\xi)=1/2\cdot\xi\cdot\gamma\cdot\sin(\theta+\beta)$, with $\xi\in[0-h_w/\sin(\theta)]$) into the comprehensive constitutive law of the single average-available-bond-length NSM FRP strip $V_{fi}\left(\bar{L}_f;\delta_{Li}\right)$. For the sake of brevity, all of the details are herein omitted but they can be found elsewhere (Bianco 2008). The equation to evaluate the maximum effective capacity $V_{fi,eff}^{\max}$ and the value of the CDC opening angle $\gamma_{\max}$ in correspondence of which it is attained, assume different features as function of the type (u) of the comprehensive constitutive law characterizing the specific case at hand.

***Cases of concrete fracture that reaches the strip's free extremity* (u = 1) *or strip tensile rupture* (u = 2)**

In these cases, the exact value of the maximum effective capacity is attained for a value of the CDC opening angle γ such as to yield an imposed end slip at the end of the crack ($\delta_{Li}(L_d)$), equal to δ_{Lu} (Fig. 9) *i.e.*:

$$V_{fi,eff}^{\max}=V_{fi,eff}(\gamma_{\max})=\frac{1}{L_d}\cdot\left\{A_1\cdot C_1^{sf}\cdot L_d^2\cdot\gamma_{\max}+\frac{A_2\cdot C_2^{sf}}{2\cdot A_3\cdot\gamma_{\max}}\cdot\right.$$
$$\left.\cdot\left[\arcsin(1-A_3\cdot\gamma_{\max}\cdot L_d)+(1-A_3\cdot\gamma_{\max}\cdot L_d)\cdot\sqrt{1-(1-A_3\cdot\gamma_{\max}\cdot L_d)^2}-\frac{\pi}{2}\right]\right\} \quad (20)$$

where:

$$A_1=-\frac{L_p\cdot J_3\cdot\lambda^3\cdot\sin(\theta+\beta)}{4\cdot\tau_0\cdot J_1};\ A_2=L_p\cdot J_3\cdot\lambda;\ A_3=\frac{\lambda^2\cdot\sin(\theta+\beta)}{2\cdot\tau_0\cdot J_1} \quad (21)$$

are integration constants independent of the type (u) of comprehensive constitutive law and:

$$\gamma_{\max}=\gamma_1=\frac{2\cdot\delta_{Lu}}{L_d\cdot\sin(\theta+\beta)} \quad (22)$$

***Case of shallow concrete fracture and strip ultimate resisting bond length smaller than the effective bond length* (*u* = 3)**

In this case, the maximum effective capacity is attained for a value of γ very close to γ_2 that is the value of the CDC opening angle such as to yield an imposed end slip at the end of the crack, equal to $\delta_{L2}\left(L_{Rfu}\right)$. For the sake of simplicity, it is assumed that $V_{fi}^{\max}$ is effectively attained for γ_2 accepting a slight approximation (Fig. 10) *i.e.*:

$$V_{fi,eff}^{\max}=\frac{1}{L_d}\cdot\left\{\left[A_1\cdot\left(C_1^{sf}-C_1\right)\cdot\left(\frac{2\cdot\delta_{L1}}{\sin(\theta+\beta)}\right)^2+\left(C_2^{sf}+C_2\right)\cdot\frac{A_2\cdot\Phi_1(\delta_{L1})}{2\cdot A_3}-\frac{A_2\cdot C_2^{sf}\cdot\pi}{4\cdot A_3}-\frac{2\cdot A_2\cdot C_1\cdot\delta_{L1}}{\sin(\theta+\beta)}\right]\cdot\frac{1}{\gamma_{\max}}+\right.$$
$$\left.-\frac{A_2\cdot C_2}{2\cdot A_3\cdot\gamma_{\max}}\cdot\left[\arcsin(1-A_3\cdot\gamma_{\max}\cdot L_d)+(1-A_3\cdot\gamma_{\max}\cdot L_d)\cdot\sqrt{1-(1-A_3\cdot\gamma_{\max}\cdot L_d)^2}\right]+A_2\cdot C_1\cdot L_d+A_1\cdot C_1\cdot\gamma_{\max}\cdot L_d^2\right\} \quad (23)$$

where A_1, A_2 and A_3 are given by Eq. (21), $\delta_{L1}=\delta_{L1}\left(L_{Rfu}\right)$ by Eq. (13) and:

$$\begin{aligned}C_1\left(L_{Rfu}\right)&=C_1^{sf}-C_1^{sf}\cdot\cos\left(\lambda\cdot L_{Rfu}\right)-C_2^{sf}\cdot\sin\left(\lambda\cdot L_{Rfu}\right)\\ C_2\left(L_{Rfu}\right)&=-C_2^{sf}-C_1^{sf}\cdot\sin\left(\lambda\cdot L_{Rfu}\right)+C_2^{sf}\cdot\cos\left(\lambda\cdot L_{Rfu}\right)\end{aligned} \quad (24)$$

$$\Phi_1(\delta_{Li})=\arcsin\left(1-\frac{2\cdot A_3\cdot\delta_{Li}}{\sin(\theta+\beta)}\right)+\left(1-\frac{2\cdot A_3\cdot\delta_{Li}}{\sin(\theta+\beta)}\right)\cdot\sqrt{1-\left(1-\frac{2\cdot A_3\cdot\delta_{Li}}{\sin(\theta+\beta)}\right)^2} \quad (25)$$

$$\gamma_{\max}=\gamma_2=\frac{2\cdot\delta_{L2}\left(L_{Rfu}\right)}{L_d\cdot\sin(\theta+\beta)} \quad (26)$$

***Case of shallow concrete fracture and strip's ultimate resisting bond length equal to the effective bond length* (*u* = 4)**

In this case, the maximum effective capacity is attained for a value of the CDC opening angle γ slightly larger than $\gamma_1=2\cdot\delta_1/(L_d\cdot\sin(\theta+\beta))$ at which the δ_1 end slip occurs at the end of the CDC (Fig. 11). Anyway, since the expressions of $V_{fi,eff}(\gamma)$ are very complex for $\gamma_1<\gamma\le\gamma_2$, instead of carrying out the derivative ($dV_{fi,eff}(\gamma)/d\gamma=0$) to search for the exact value of $\gamma_{\max}$, it is deemed reasonable to assume γ_1 as the angle where the maximum effective capacity occurs. The solution so obtained, slightly underestimating the real maximum, is:

$$V_{fi,eff}^{\max}=\frac{1}{L_d}\cdot\left\{A_1\cdot C_1^{sf}\cdot L_d^2\cdot\gamma_{\max}+\frac{A_2\cdot C_2^{sf}}{2\cdot A_3\cdot\gamma_{\max}}\cdot\right.$$
$$\left.\cdot\left[\arcsin(1-A_3\cdot\gamma_{\max}\cdot L_d)+(1-A_3\cdot\gamma_{\max}\cdot L_d)\cdot\sqrt{1-(1-A_3\cdot\gamma_{\max}\cdot L_d)^2}-\frac{\pi}{2}\right]\right\} \tag{27}$$

where A_1, A_2 and A_3 are given by Eq. (21) and:

$$\gamma_{\max}=\gamma_1=\frac{2\cdot\delta_1}{L_d\cdot\sin(\theta+\beta)} \tag{28}$$

***Case of shallow concrete fracture and strip's ultimate resisting bond length larger than the effective bond length* (*u* = 5)**

In this case, the maximum effective capacity is attained for a value of the CDC opening angle γ slightly larger than $\gamma_2=2\cdot\delta_{L2}/(L_d\cdot\sin(\theta+\beta))$ at which the end slip $\delta_{L2}\left(L_{Rfu}\right)$ occurs at the end of the CDC (Fig. 12). Again, since the expressions of $V_{fi,eff}(\gamma)$ are very complex for $\gamma_2<\gamma\le\gamma_3$, it is deemed a reasonable compromise between accuracy of prediction and computational demand, to assume γ_2 as the angle in correspondence of which the maximum effective capacity occurs. The solution so obtained, slightly underestimating the real maximum, is:

$$V_{fi,eff}^{\max}=\frac{1}{L_d}\cdot\left\{\left[A_1\cdot C_1^{sf}\cdot\left(\frac{2\cdot\delta_1}{\sin(\theta+\beta)}\right)^2+\frac{C_2^{sf}\cdot A_2\cdot\Phi_1(\delta_1)}{2\cdot A_3}-\frac{A_2\cdot C_2^{sf}\cdot\pi}{4\cdot A_3}\right]\cdot\frac{1}{\gamma_{\max}}+V_{f1}^{bd}\cdot\left(L_d-\frac{2\cdot\delta_1}{\gamma_{\max}\cdot\sin(\theta+\beta)}\right)\right\} \tag{29}$$

where A_1, A_2 and A_3 are given by Eq. (21), $\Phi_1(\delta_1)$ as given by Eq. (25) and:

$$\gamma_{\max}=\gamma_2=\frac{2\cdot\delta_{L2}\left(L_{Rfu}\right)}{L_d\cdot\sin(\theta+\beta)} \tag{30}$$

***Case of deep concrete fracture* (*u* = 6)**

In this case, it is not known *a priori* if the maximum effective capacity is attained at a value of the CDC opening angle such as to yield an imposed end slip at the end of the crack, equal to δ_{Lu} or to $\delta_{L2}\left(L_{Rfu}\right)$ (Fig. 13). Thus, the maximum effective capacity will be given by:

$$V_{fi,eff}^{\max}=\max\left\{V_{fi,eff}^{\max 1};V_{fi,eff}^{\max 2}\right\} \tag{31}$$

where:

$$V_{fi,eff}^{\max 1} = V_{fi,eff}(\gamma_{\max 1}) = \frac{1}{L_d} \cdot \left\{ A_1 \cdot C_1^{sf} \cdot L_d^2 \cdot \gamma_{\max 1} + \frac{A_2 \cdot C_2^{sf}}{2 \cdot A_3 \cdot \gamma_{\max 1}} \cdot \right.$$
$$\left. \cdot \left[\arcsin(1 - A_3 \cdot \gamma_{\max 1} \cdot L_d) + (1 - A_3 \cdot \gamma_{\max 1} \cdot L_d) \cdot \sqrt{1 - (1 - A_3 \cdot \gamma_{\max 1} \cdot L_d)^2} - \frac{\pi}{2} \right] \right\} \tag{32}$$

$$\gamma_{\max 1} = \gamma_1 = \frac{2 \cdot \delta_{Lu}}{L_d \cdot \sin(\theta + \beta)} \tag{33}$$

and:

$$V_{fi,eff}^{\max 2} = V_{fi,eff}(\gamma_{\max 2}) =$$
$$\frac{1}{L_d} \cdot \left\{ \left[A_1 \cdot \left(C_1^{sf} - C_1 \right) \cdot \left(\frac{2 \cdot \delta_{Lu}}{\sin(\theta + \beta)} \right)^2 + \left(C_2^{sf} + C_2 \right) \cdot \frac{A_2 \cdot \Phi_1(\delta_{Lu})}{2 \cdot A_3} - \frac{A_2 \cdot C_2^{sf} \cdot \pi}{4 \cdot A_3} - \frac{2 \cdot A_2 \cdot C_1 \cdot \delta_{Lu}}{\sin(\theta + \beta)} \right] \cdot \frac{1}{\gamma_{\max 2}} + \right. \tag{34}$$
$$\left. - \frac{A_2 \cdot C_2}{2 \cdot A_3 \cdot \gamma_{\max 2}} \cdot \left[\arcsin(1 - A_3 \cdot \gamma_{\max 2} \cdot L_d) + (1 - A_3 \cdot \gamma_{\max 2} \cdot L_d) \cdot \sqrt{1 - (1 - A_3 \cdot \gamma_{\max 2} \cdot L_d)^2} \right] + A_2 \cdot C_1 \cdot L_d + A_1 \cdot C_1 \cdot \gamma_{\max 2} \cdot L_d^2 \right\}$$

$$\gamma_{\max 2} = \gamma_2 = \frac{2 \cdot \delta_{L2}\left(L_{Rfu}\right)}{L_d \cdot \sin(\theta + \beta)} \tag{35}$$

and where A_1, A_2 and A_3 are given by Eq. (21), $C_1\left(L_{Rfu}\right)$ and $C_2\left(L_{Rfu}\right)$ as given by Eq. (24) and $\Phi_1(\delta_{Lu})$ as given by Eq. (25).

Actual and Design value of the Shear Strengthening Contribution

The actual V_f and design value V_{fd} of the NSM shear strength contribution, can be obtained as follows:

$$V_{fd} = \frac{1}{\gamma_{Rd}} \cdot V_f = \frac{1}{\gamma_{Rd}} \cdot \left(2 \cdot N_{f,\text{int}}^{l} \cdot V_{fi,eff}^{\max} \cdot \sin\beta \right) \tag{36}$$

where γ_{Rd} is the partial safety factor, divisor of a capacity, that can be assumed as 1.1-1.2 according to the level of uncertainty affecting the input parameters but, in this respect, a reliability-based calibration is needed.

Model Appraisal

The proposed model was applied to the RC beams tested by Dias and Barros (2008), by Dias *et al.* (2007) and by Dias (2008). The beams tested in the first two experimental programs (series I and II) were T cross-section RC beams characterized by the same test set-up with the same ratio between the shear span and the beam effective depth ($a/d = 2.5$), the same amount of longitudinal reinforcement, the same kind of CFRP strips and epoxy adhesive and they differed for the concrete mechanical properties. In fact, the first experimental program (series I) was characterized by a concrete average compressive strength f_{cm} of 31.1 *MPa*, while the second (series II) by 18.6 *MPa*. Both series presented different configurations of NSM strips, in terms of both inclination β and

spacing s_f. The first program also included beams characterized by a different amount of existing steel stirrups (see Table 1). The beams tested in the third experimental program (series III) were characterized by the same test set up, but with a different shear aspect ratio ($a/d = 3.3$) and distinct concrete mechanical properties ($f_{cm} = 59.4\ MPa$). Some of them were also subjected to pre-cracking (their label includes a letter F). The details of the beams taken to appraise the predictive performance of the developed model are listed in Table 1. Those beams are characterized by the following common geometrical and mechanical parameters: $b_w = 180\ mm$; $h_w = 300\ mm$; $f_{fu} = 2952\ MPa$ (for the series I and II) and $f_{fu} = 2848\ MPa$ (for the series III); $E_f = 166.6\ GPa$ (for the series I and II) and $E_f = 174.3\ GPa$ (for the series III); $a_f = 1.4\ mm$; $b_f = 10.0\ mm$. The CDC inclination angle θ adopted in the simulations, listed in Table 1 for all the beams analyzed, is the one experimentally observed by inspecting the crack patterns (Dias 2008). Note that the experimental observations confirm the expected trend according to which θ diminishes for increasing values of the ratio a/d (*e.g.* Bousselham and Chaalal 2004, Chao *et. al.* 2005). In fact, for some beams of the III series ($a/d = 3.3$), $\theta^{\exp}$ assumes values smaller than 45º and up to 20º (Table 1). In this respect, it has to be stressed that assuming $\theta = 45^{\circ}$ can result excessively conservative since, with respect to smaller values (*e.g.* $\theta = 20^{\circ}$), and other parameters being the same, the predicted NSM shear strength contribution decreases due to the fact that the number of strips effectively crossing the CDC diminishes (Bianco 2008). It would be necessary to develope rigorous equations to evaluate the CDC inclination angle θ as function of 1) shear aspect ratio a/d and amount of both 2) NSM strips and 3) existing steel stirrups but, in this respect, further research is necessary. The angle α was assumed equal to 28.5°, being the average of values obtained in a previous investigation (Bianco *et al.* 2006) by back-analysis of experimental data. As to the value of α, due to its importance to the prediction accuracy of NSM shear strength contributions, further research is desirable. The parameter characterizing the loading process is: $\dot{\delta}_{Li} = 0.0001\ rads$. Concrete average tensile strength f_{ctm} was calculated from the average compressive strength by means of the formulae of the CEB Fib Model Code 1990 resulting in 2.45 *MPa*, 1.45 *MPa* and 4.17 *MPa* for the series I, II and III, respectively. The parameters characterizing the adopted local bond stress-slip relationship (Fig. 1b) are: $\tau_0 = 20.1\ MPa$ and $\delta_1 = 7.12\ mm$. Those values were obtained by the values characterizing the more sophisticated local bond stress-slip relationship adopted in previous works (Bianco *et al.* 2009a, 2010), by fixing the value of $\tau_0 = 20.1\ MPa$ and determining $\delta_1 = 7.12\ mm$ by equating the fracture energy. In this respect, it has to be underlined that the necessity is felt to

develop rigorous equations that would allow the values (τ_0, δ_1) characterizing the local bond stress slip relationship to be determined on the basis of: a) superficial chemical and micro-mechanical properties of FRP, adhesive and concrete, and b) the adhesive layer thickness. Nonetheless, further research is, in this respect, required. However, as highlighted by means of parametric studies (Bianco 2008), for the values of concrete mechanical properties that can be met in practice, debonding rarely occurs due the high capacity of currently available structural adhesives. Thus, slight variations of the values of the parameters τ_0 and δ_1 can not be felt, in terms of NSM shear strength contribution, due to the premature occurrence of other failure modes such as either concrete fracture or strip rupture. For this reason, adopting values of $\tau_0 = 20.1\,MPa$ and $\delta_1 = 7.12\,mm$ for cases characterized by different values of both 1) superficial chemical-mechanical properties of FRP, adhesive and concrete, and 2) adhesive thickness, is not expected to significantly affect the predictive performance of the model.

Table 1 shows that the model, in general, provides reasonable underestimates of the experimental recordings $V_f^{\exp}$ since the ratio $V_f / V_f^{\exp}$ presents mean value and standard deviation equal to 0.86 and 0.33, respectively. The values of NSM shear strength contribution have also been compared with the maximum values provided by the more refined model in correspondence of three different geometrical configurations that the occurred CDC could assume with respect to the strip ($V_{f,1}^{\max}$, $V_{f,2}^{\max}$ and $V_{f,3}^{\max}$ in Table 1). The simplified model herein presented, in some cases (*e.g.* beam 2S-5LV-I) provides a value of the NSM shear strength contribution that lies in between the minimum and maximum values obtained by the more refined model and in other cases (*e.g.* 2S-5LI45-I) it gives a value that is rather lower than the lower bound of the values obtained by the more refined model. This is reasonable, since the approximations introduced inevitably reduce the accuracy.

The model herein proposed, as the more refined one, both seem to provide reasonable estimates of the experimental recordings regardless of the amount of existing stirrups. Actually, the authors think that the amount of existing stirrups affects the depth to which the concrete fracture can penetrate the beam web core but, since it also affects the CDC inclination angle $\theta^{\exp}$, both models end up giving satisfactory results regardless of the amount of existing stirrups (Table 1). Anyway, in this respect, further research is needed.

Conclusions

A closed-form computational procedure to evaluate the NSM FRP strips shear strength contribution to RC beams was developed by simplifying a more sophisticated model recently developed. That procedure was obtained by

introducing some substantial simplifications, such as: 1) assuming a simplified local bond stress-slip relationship, 2) taking into consideration the average-available-bond-length NSM FRP strip confined to a concrete prism, and 3) assuming the concrete fracture surfaces as being semi-pyramidal instead of semi-conical. Given those simplifications, the procedure is based on 1) the evaluation of the constitutive law of the average-available-bond-length strip and 2) the determination of the maximum effective capacity that this latter can provide during the loading process of the strengthened beam, once the kinematic mechanism has been suitably imposed. The estimates of the NSM shear strength contribution obtained by means of that simplified model showed a reasonable agreement with both the experimental recordings and the predictions obtained by a more sophisticated model. Anyway, the introduction of substantial simplifications inevitably brought a loss of accuracy. Moreover, many aspects such as: 1) the correct evaluation of the local bond stress slip relationship as function of both the chemical-mechanical properties of FRP, concrete and adhesive and this latter thickness; 2) the correct evaluation of the CDC inclination angle as function of shear aspect ratio and amount of both FRPs and existing steel stirrups; and 3) the issue of the interaction with existing stirrups, still have to be addressed.

Acknowledgements

The authors of the present work wish to acknowledge the support provided by the "Empreiteiros Casais", S&P®, degussa® Portugal, and Secil (Unibetão, Braga). The study reported in this paper forms a part of the research program "CUTINEMO - Carbon fiber laminates applied according to the near surface mounted technique to increase the flexural resistance to negative moments of continuous reinforced concrete structures" supported by FCT, PTDC/ECM/73099/2006. Also, this work was carried out under the auspices of the Italian DPC-ReLuis Project (repertory n. 540), Research Line 8, whose financial support is greatly appreciated.

Notation

A_c = area of the concrete prism cross section

A_f = area of the strip's cross section

A_1 = integration constant entering the expressions to evaluate the $V_{fi,eff}^{\max}$

A_2 = integration constant entering the expressions to evaluate the $V_{fi,eff}^{\max}$

A_3 = integration constant entering the expressions to evaluate the $V_{fi,eff}^{\max}$

C_1^{sf} = first integration constant for the softening friction phase

C_2^{sf} = second integration constant for the softening friction phase

$C_1\left(L_{Rfi}\right)$ = resisting-bond-length-dependent integration term

$C_2\left(L_{Rfi}\right)$ = resisting-bond-length-dependent integration term

E_c = concrete Young's modulus

E_f = strips' CFRP Young's modulus

J_1 = bond modeling constant

J_2 = bond modeling constant

J_3 = bond modeling constant

L_d = CDC length

L_f = Actual length of th strips

L_{fi} = *i*-th strip available bond length

$\bar{L}_f$ = average available bond length

$L_{fi}^c\left(t_n;q_n\right)$ = height of the concrete semi-pyramid in correspondence of the *i*-th strip

L_p = effective perimeter of the strip cross section

$L_{Rfi}\left(t_n;q_n\right)$ = *i*-th strip resisting bond length

$L_{tr,\,fi}\left(L_{Rfi};\delta_{Li}\right)$ = transfer length of the *i*-th strip for the relevant imposed slip

$L_{tr}^{bd}\left(\delta_{Li}\right)$ = necessary bond transfer length

$L_{tr,fi}^{bd}\left(L_{Rfi};\delta_{Li}\right)$ = bond based transfer length of the *i*-th strip for the relevant imposed slip

L_{tr1} = maximum invariant value of transfer length that can undergo elastic phase

$L_{tr}^{fs}\left(\delta_{Li}\right)$ = amount of a transfer length for an infinite bond length undergoing free slipping

$L_{tr}^{sf}\left(\delta_{Li}\right)$ = softening frictional amount of a transfer length for an infinite bond length

$N_{f,\text{int}}^{l}$ = minimum integer number of strips that can effectively cross the CDC

$OXYZ$ = crack plane reference system

$O_i^l X_i^l$ = reference axis along the *i*-th strip available bond length L_{fi}

V_{fi}^{cf} = progressive concrete tensile fracture capacity along the *i*-th strip

V_1^{db} = value of force transferred by bond along the elastic transfer length L_{tr1}

$V_{fi}^{\max}$ = maximum effective capacity

$V_f^{\exp}$ = experimental value of the NSM shear strengthening contribution

V_f = actual value of the NSM shear strengthening contribution

V_{fd} = design value of the NSM shear strengthening contribution

$V_{fi,CDC}(\xi;\gamma)$ = distribution of the NSM strip capacity along the CDC

$V_{fi}\left(\overline{L}_f;\delta_{Li}\right)$ = comprehensive constitutive law of the average available bond length

$V_{fi}^{bd}\left(\overline{L}_f;\delta_{Li}\right)$ = bond-based constitutive law of the average available bond length

a_c = concrete prismatic specimen thickness

a_f = strip cross section's thickness

b_c = concrete prismatic specimen width

b_f = strip cross section's width

b_w = beam cross section's width

f_{cm} = concrete average compressive strength

f_{ctm} = concrete average tensile strength

f_{fu} = FRP strip tensile strength

h_w = beam web height

i = strips counter

$o^{fs}x^{fs}$ = reference axis along the amount of the infinite strip in free slipping phase

$o^{sf}x^{sf}$ = reference axis along the amount of the infinite strip in softening friction phase

$o_i^{tr}x_i^{tr}$ = reference axis along the strip's transfer length

q_e = iteration in correspondence of which equilibrium is attained

q_m = m-th iteration

s_f = Spacing between adjacent strips along the CDC axis

t_0 = load step of formation of the critical diagonal crack

t_1 = load step at which the critical diagonal crack starts widening

t_n = generic n-th load step

t_s = slab thickness

u = parameter defining the comprehensive constitutive law type

x_{fi} = position of the *i*-th strip along the global reference system

$\Phi_1(\delta_{Li})$ = Imposed-end-slip-dependent expression

α = angle defining the concrete fracture surface

β = FRP strips inclination angle with respect to the beam longitudinal axis

$\delta(x)$ = slip along the strip's length

δ_1 = slip corresponding to the end of softening friction

δ_{Li} = imposed slip at the loaded extremity of the *i*-th strip

$\dot{\delta}_{Li}$ = imposed slip increment

$\delta_{L1}(L_{Rfi})$ = value of δ_{Li} defining the end of the first phase of the bond-based constitutive law

$\delta_{L2}(L_{Rfi})$ = value of δ_{Li} defining the end of the second phase of the bond-based constitutive law

$\delta_{L3}(L_{Rfi})$ = value of δ_{Li} defining the end of the third phase of the bond-based constitutive law

$\gamma(t_n)$ = critical diagonal crack opening angle

γ_1 = CDC opening angle such that the imposed end slip at L_d is equal to δ_{L1}

γ_2 = CDC opening angle such that the imposed end slip at L_d is equal to δ_{L2}

γ_3 = CDC opening angle such that the imposed end slip at L_d is equal to δ_{L3}

$\gamma_{\max}$ = CDC opening angle for which the maximum effective capacity is attained

γ_{Rd} = partial safety factor divisor of the capacity

λ = constant entering the governing differential equation for elastic phase

θ = critical Diagonal Crack (CDC) inclination angle

$\theta^{\exp}$ = experimentally observed CDC inclination angle

$\tau(\delta)$ = local bond stress-slip relationship

$\tau(x)$ = bond stress along the strip length

τ_0 = adhesive-cohesive initial bond strength

ξ = reference axis along the CDC

References

Bianco, V., Barros, J.A.O., Monti, G., (2006). "Shear Strengthening of RC beams by means of NSM laminates: experimental evidence and predictive models", Technical report 06-DEC/E-18, Dep. Civil Eng., School Eng. University of Minho, Guimarães- Portugal.

Bianco, V., Barros, J.A.O., Monti, G., (2007). "Shear Strengthening of RC beams by means of NSM strips: a proposal for modeling debonding", Technical report 07-DEC/E-29, Dep. Civil Eng., School Eng. University of Minho, Guimarães- Portugal.

Bianco, V., Barros, J.A.O., Monti, G., (2009a). "Three dimensional mechanical model for simulating the NSM FRP strips shear strength contribution to RC beams", Engineering Structures, 31(4), April 2009, 815-826.

Bianco, V., Barros, J.A.O., Monti, G., (2009b). "Bond Model of NSM FRP strips in the context of the Shear Strengthening of RC beams", ASCE Journal of Structural Engineering, 135(6), June 2009.

Bianco, V., Barros, J.A.O., Monti, G., (2010). "New approach for modeling the contribution of NSM FRP strips for shear strengthening of RC beams", ASCE Journal of Composites for Construction, 14(1), January/February 2010.

Bianco, V., (2008). "Shear Strengthening of RC beams by means of NSM FRP strips: experimental evidence and analytical modeling", PhD Thesis, Dept. of Structural Engrg. and Geotechnics, Sapienza University of Rome, Italy, submitted on December 2008.

Bousselham A., Chaalal O., (2004) "Shear Strengthening Reinforced Concrete Beams with Fiber-Reinforced Polymer: Assessment of Influencing Parameters and Required Research", ACI Structural Journal, Vol.101, Nº2, March-April, pp. 219-227.

CEB-FIP Model Code 90, (1993) Bulletin d'Information N° 213/214, Final version printed by Th. Telford, London, (1993; ISBN 0-7277-1696-4; 460 pages).

Chao S.Y., Chen J.F., Teng J.G., Hao Z., Chen J., (2005) "Debonding in Reinforced Concrete Beams Shear Strengthened with Complete Fiber Reinforced Polymer Wraps", Journal of Composites for Construction, ASCE September/October 2005/1.

Dias, S.J.E. (2008). "Experimental and anlytical research in the shear strengthening of reinforced concreet beams using the near surface mounted technique with CFRP strips", PhD Thesis, Department of Civil Engineering, University of Minho, Guimarães-Portugal, in Portuguese.

Dias, S.J.E., Bianco, V., Barros, J.A.O., Monti, G., (2007). "Low strength concrete T cross section RC beams strengthened in shear by NSM technique", Workshop-Materiali ed Approcci Innovativi per il Progetto in

Zona Sismica e la Mitigazione della Vulnerabilità delle Strutture, University of Salerno, Italy, 12-13 February.

Dias, S.J.E. and Barros, J.A.O., (2008). “Shear Strengthening of T Cross Section Reinforced Concrete Beams by Near Surface Mounted Technique”, Journal of Composites for Construction, ASCE, Vol. 12, No. 3, pp. 300-311.

Monti, G., Renzelli, M., Luciani, P., (2003) “FRP Adhesion to Uncracked and Cracked Concrete Zones”, Proceedings of the 6th International Symposium on Fibre-Reinforced Polymer (FRP) Reinforcement for Concrete Structures (FRPRCS-6), Singapore, July, 183-192.

Monti, G., Santinelli, F., Liotta, M.A., (2004) “Mechanics of FRP Shear Strengthening of RC beams”, Proc. ECCM 11, Rhodes, Greece.

Monti, G., Liotta, M.A., (2007) “Tests and design equations for FRP-strengthening in shear”, Construction and Building Materials (2006), 21(4), April 2007, 799-809.

Mohammed Ali, M.S., Oehlers, D.J., Seracino, R. (2006). “Vertical shear interaction model between external FRP transverse plates and internal stirrups”, Engineering Structures 28, 381-389.

Mohammed Ali, M.S., Oehlers, D.J., Griffith, M.C., Seracino, R. (2007). “Interfacial stress transfer of near surface-mounted FRP-to-concrete joints”, Engineering Structures 30, 1861-1868.

Rizzo, A. and De Lorenzis, L., (2009) “Behaviour and capacity of Rc beams strengthened in shear with NSM FRP reinforcement”, Construction and Building Materials, Vol. 3, n. 4, April 2009, 1555-1567.

Sekulic, A., Curnier, A., (2006). “An original epoxy-stamp on glass-disc specimen exhibiting stable debonding for identifying adhesive properties between glass and epoxy”, International Journal of Adhesion and Adhesives, Vol. 27, pp. 611-620.

Sena-Cruz, J.M., Barros, J.A.O., (2004). “Bond between near-surface mounted CFRP laminate strips and concrete in structural strengthening”, Journal of Composites for Construction, ASCE, Vol. 8, No. 6, pp. 519-527.

Yuan, H., Teng, J.G., Seracino, R., Wu, Z.S., Yao, J. (2004). “Full-range behavior of FRP-to-concrete bonded joints”, Engineering Structures, 26, 553-565.

Zhai, L.L., Ling, G.P., Wang, Y.W., (2008). “Effect of nano-Al_2O_3 on adhesion strength of epoxy adhesive and steel”, International Journal of Adhesion and Adhesives, Vol. 28, No. 1-2, pp. 23-28.

TABLE CAPTIONS

Table 1. Values of the parameters characterizing the beams adopted to appraise the formulation proposed.

Table 1. Values of the parameters characterizing the beams adopted to appraise the formulation proposed.

Beam Label	θ^{exp} °	β °	s_f *mm*	Steel Stirrups	$V_{f,1}^{max}$ *kN*	$V_{f,2}^{max}$ *kN*	$V_{f,3}^{max}$ *kN*	V_f^{exp} *kN*	$\bar{L}_f$ *mm*	u	V_f *kN*
2S-3LV-I	40	90	267	ϕ6/300	18.53	6.46	55.33	**22.20**	75.96	3	**10.77**
2S-5LV-I	40	90	160	"	52.33	26.42	55.34	**25.20**	82.87	6	**30.97**
2S-8LV-I	36	90	100	"	68.58	58.88	64.33	**48.60**	77.34	3	**29.59**
2S-3LI45-I	45	45	367	"	35.10	15.41	45.73	**29.40**	164.75	3	**23.44**
2S-5LI45-I	45	45	220	"	46.11	49.14	45.74	**41.40**	134.35	3	**23.19**
2S-8LI45-I	36	45	138	"	75.89	79.71	78.73	**40.20***	106.73	6	**59.55**
2S-3LI60-I	33	60	325	"	50.69	18.90	51.68	**35.40**	169.16	3	**30.74**
2S-5LI60-I	36	60	195	"	36.37	36.59	48.55	**46.20**	77.27	6	**22.27**
2S-7LI60-I	33	60	139	"	52.98	63.07	67.58	**54.60**	91.05	6	**60.80**
2S-7LV-II	46	90	114	ϕ6/300	26.72	31.84	35.59	**28.32**	90.97	6	**15.04**
2S-4LI45-II	40	45	275	"	25.06	21.89	37.30	**33.90**	123.41	3	**19.24**
2S-7LI45-II	30	45	157	"	49.36	47.13	45.95	**48.00**	108.27	6	**37.92**
2S-4LI60-II	40	60	243	"	21.31	15.04	29.38	**33.06**	93.90	3	**13.23**
2S-6LI60-II	27	60	162	"	42.79	37.54	39.45	**42.72**	99.56	6	**34.68**
4S-7LV-II	46	90	114	ϕ6/180	26.72	31.84	35.59	**6.90***	90.97	6	**15.04**
4S-4LI45-II	40	45	275	"	25.06	21.89	37.30	**26.04**	123.41	3	**19.24**
4S-7LI45-II	40	45	157	"	40.58	37.48	40.63	**31.56**	110.83	6	**28.36**
4S-4LI60-II	40	60	243	"	21.31	15.04	29.38	**25.08**	93.90	3	**13.23**
4S-6LI60-II	30	60	162	"	38.92	35.46	36.71	**35.10**	92.20	3	**25.72**
3S-5LI45-III	30	45	275	ϕ6/300	59.74	59.55	70.01	**66.10**	140.95	3	**70.33**
3S-5LI45F1-III**	23	45	275	"	83.05	86.96	81.15	**85.75**	128.32	3	**77.93**
3S-5LI45F2-III**	30	45	275	"	59.74	59.55	70.01	**65.35**	140.95	3	**70.33**
5S-5LI45-III	28	45	275	ϕ6/200	78.24	59.55	72.01	**74.90**	102.84	3	**57.76**
5S-5LI45F-III**	28	45	275	"	78.24	59.55	72.01	**74.90**	102.84	3	**57.76**
3S-9LI45-III	32	45	157	ϕ6/300	109.88	109.32	98.30	**101.85**	126.75	6	**114.30**
5S-9LI45-III	32	45	157	ϕ6/200	109.88	109.32	98.30	**108.90**	126.75	6	**114.30**
3S-5LI60-III	26	60	243	ϕ6/300	71.74	76.20	62.81	**69.00**	88.56	3	**52.84**
5S-5LI60-III	25	60	243	ϕ6/200	68.48	77.44	63.79	**73.35**	93.49	3	**59.82**
5S-5LI60F-III**	25	60	243	"	68.48	77.44	63.79	**72.55**	93.49	3	**59.82**
3S-8LI60-III	22	60	162	ϕ6/300	112.82	119.58	112.25	**112.30**	97.54	3	**109.30**
5S-8LI60-III	19	60	162	ϕ6/200	123.34	122.74	132.00	**122.45**	92.61	3	**114.69**
3S-6LV-III	45	90	180	ϕ6/300	58.24	26.62	66.53	**39.58**	120.00	6	**35.04**
3S-10LV-III	32	90	114	"	97.50	82.41	85.21	**83.25**	78.76	3	**60.23**

I) beams tested by Dias & Barros (2006) and characterized by *a/d* equal to 2.5 and f_{cm} equal to 31.1 *MPa*; II) beams tested by Dias *et al.* (2007) and characterized by *a/d* equal to 2.5 and f_{cm} equal to 18.6 *MPa*; III) beams tested by Dias (2008) and characterized by *a/d* equal to 3.3 and f_{cm} equal to 59.4 *MPa*.

* beams whose experimental value of NSM shear strength contribution is affected by some disturbance;

** beams which were subjected to pre-cracking.

FIGURE CAPTIONS

Fig. 1. Main physical-mechanical features of the theoretical model and calculation procedure: a) average-available-bond-length NSM strip and relevant prism of surrounding concrete, b) adopted local bond stress-slip relationship, c) NSM strip confined to the corresponding prism of surrounding concrete and semi-pyramidal fracture surface, d) sections of the concrete prism.

Fig. 2. Calculation procedure: main algorithm.

Fig. 3. Determination of bond-based constitutive law $V_{fi}^{bd}\left(\delta_{Li};L_{Rfi}\right)$ and bond transfer length $L_{tr,fi}^{bd}\left(\delta_{Li};L_{Rfi}\right)$: (a) invariant distribution of bond shear stress $\tau(x)$ and slip $\delta(x)$ for an infinite value of L_{Rfi} and (b-g) singling out of the three bond phases and relative limits ($\delta_{Li}\left(L_{Rfi}\right)\, i=1,2,3$) as a result of the progressive migration of $\tau(x)$ from the Loaded End (LE) towards the Free End (FE) for whatever value of L_{Rfi} and by increasing δ_{Li}.

Fig. 4. Bond-based constitutive law of a single NSM FRP strip: (a) relationship between the bond transfer length $L_{tr,fi}^{bd}\left(\delta_{Li};L_{Rfi}\right)$ and the imposed end slip δ_{Li} for different values of resisting bond length L_{Rfi}; (b) bi-dimensional and (c) three-dimensional representation of the relationship between the force transferrable by bond $V_{fi}^{bd}\left(\delta_{Li};L_{Rfi}\right)$ and δ_{Li} for different values of L_{Rfi}.

Fig. 5. Determination of the comprehensive constitutive law: flow chart.

Fig. 6. Single NSM FRP strip comprehensive constitutive law in the case in which concrete fracture remains shallow: a) resulting constitutive law $V_{fi}\left(\bar{L}_{fi};\delta_{Li}\right)$ in a bi-dimensional representation, b) resulting overall transfer length $L_{tr,fi}\left(\bar{L}_{fi};\delta_{Li}\right)$, c) section of the concrete prism and occurrence of subsequent fractures and d) resulting constitutive law $V_{fi}\left(\bar{L}_{fi};\delta_{Li}\right)$ in a three-dimensional representation. Note that this plot has been done for an initial resisting bond length equal to the effective bond length but this does not affect the generality of the exposition.

Fig. 7. Single NSM FRP strip comprehensive constitutive law in the case in which concrete fracture is deep: a) resulting constitutive law $V_{fi}\left(\bar{L}_{fi};\delta_{Li}\right)$ in a bi-dimensional representation, b) resulting overall transfer length $L_{tr,fi}\left(\bar{L}_{fi};\delta_{Li}\right)$, c) section of the concrete prism and occurrence of subsequent fractures and d) resulting constitutive law $V_{fi}\left(\bar{L}_{fi};\delta_{Li}\right)$ in a three-dimensional representation. Note that this plot has been done for an

initial resisting bond length equal to the effective bond length but this does not affect the generality of the exposition.

Fig. 8. Possible comprehensive constitutive law of an NSM CFRP strip confined within a prism of concrete: (a) concrete that reaches the inner tip ($u=1$) or strip tensile rupture ($u=2$), (b) superficial and/or absent concrete fracture and ultimate resisting bond length smaller ($u=3$) or equal ($u=4$) to the effective bond length, (c) superficial and/or absent concrete fracture and ultimate resisting bond length larger ($u=5$) than the effective bond length and (d) deep concrete fracture ($u=6$).

Fig. 9. Maximum effective capacity along the CDC for the cases of concrete fracture that reaches the inner tip ($u=1$) or strip's tensile rupture ($u=2$): a) capacity $V_{fi,CDC}(\gamma;\xi)$ and c) imposed end slip $\delta_{Li,CDC}(\gamma;\xi)$ distribution along the CDC for different values of the CDC opening angle γ, b) comprehensive constitutive law and d) effective capacity as function of the CDC opening angle γ.

Fig. 10. Maximum effective capacity along the CDC for the case of shallow concrete fracture and an ultimate value of the resisting bond length smaller than the effective bond length ($u=3$): a) capacity $V_{fi,CDC}(\gamma;\xi)$ and c) imposed end slip $\delta_{Li,CDC}(\gamma;\xi)$ distribution along the CDC for different values of the CDC opening angle γ, b) comprehensive constitutive law and d) effective capacity as function of the CDC opening angle γ.

Fig. 11. Maximum effective capacity along the CDC for the case of shallow concrete fracture and an ultimate value of the resisting bond length equal to the effective bond length ($u=4$): a) capacity $V_{fi,CDC}(\gamma;\xi)$ and c) imposed end slip $\delta_{Li,CDC}(\gamma;\xi)$ distribution along the CDC for different values of the CDC opening angle γ, b) comprehensive constitutive law and d) effective capacity as function of the CDC opening angle γ.

Fig. 12. Maximum effective capacity along the CDC for the case of shallow concrete fracture and an ultimate value of the resisting bond length larger than the effective bond length ($u=5$): a) capacity $V_{fi,CDC}(\gamma;\xi)$ and c) imposed end slip $\delta_{Li,CDC}(\gamma;\xi)$ distribution along the CDC for different values of the CDC opening angle γ, b) comprehensive constitutive law and d) effective capacity as function of the CDC opening angle γ.

Fig. 13. Maximum effective capacity along the CDC for the case of deep concrete fracture ($u=6$): a) capacity $V_{fi,CDC}(\gamma;\xi)$ and c) imposed end slip $\delta_{Li,CDC}(\gamma;\xi)$ distribution along the CDC for different values of the CDC opening angle γ, b) comprehensive constitutive law and d) effective capacity as function of the CDC opening angle γ.

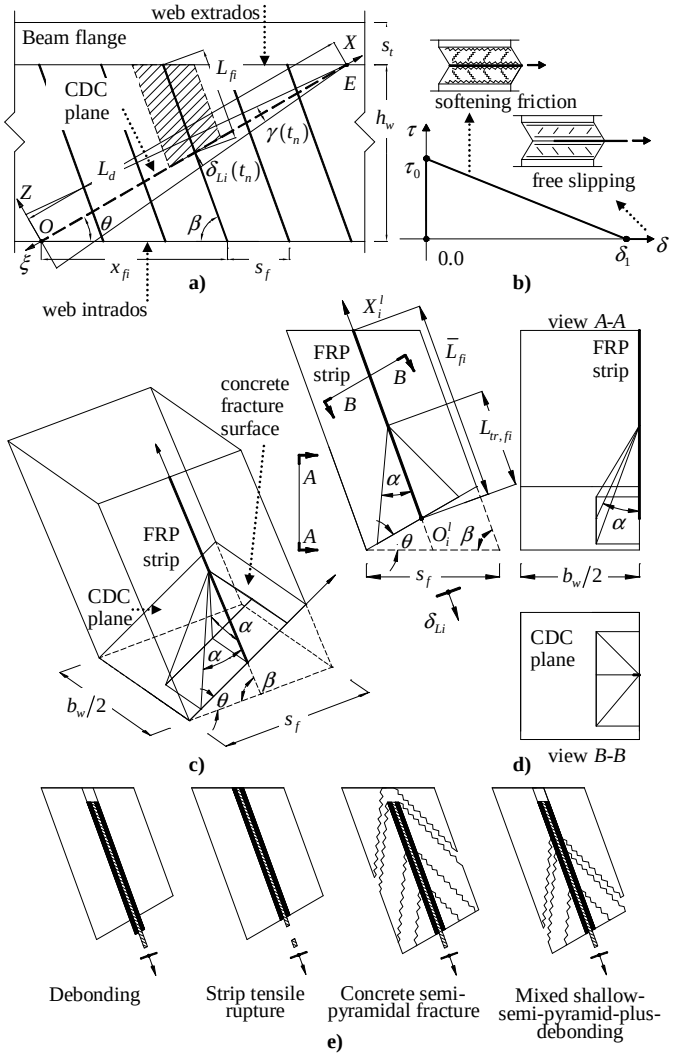

Fig. 1. Main physical-mechanical features of the theoretical model and calculation procedure: a) average-available-bond-length NSM strip and relevant prism of surrounding concrete, b) adopted local bond stress-slip relationship, c) NSM strip confined to the corresponding concrete prism of surrounding concrete and semi-pyramidal fracture surface, d) sections of the concrete prism.

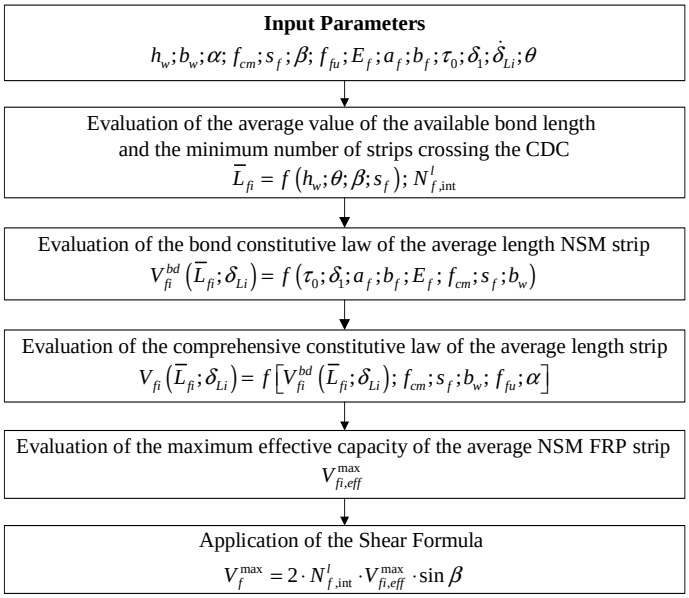

Fig. 2. Calculation procedure: main algorithm.

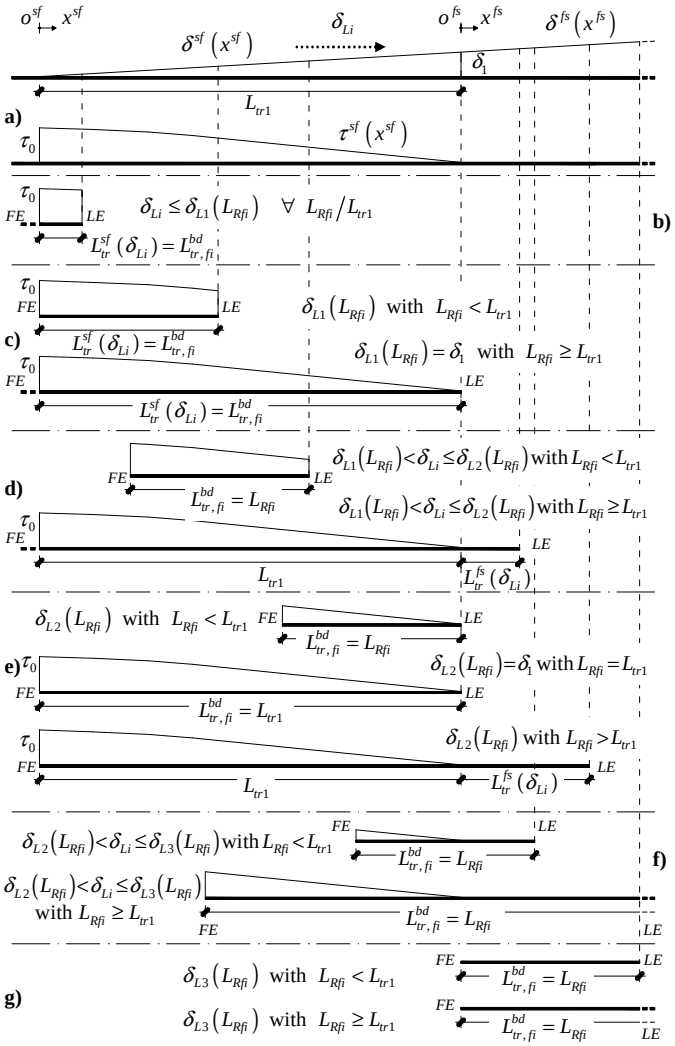

Fig. 3. Determination of bond-based constitutive law $V_{fi}^{bd}\left(\delta_{Li};L_{Rfi}\right)$ and bond transfer length $L_{tr,fi}^{bd}\left(\delta_{Li};L_{Rfi}\right)$: (a) invariant distribution of bond shear stress $\tau(x)$ and slip $\delta(x)$ for an infinite value of L_{Rfi} and (b-g) singling out of the three bond phases and relative limits ($\delta_{Li}\left(L_{Rfi}\right)\, i=1,2,3$) as a result of the progressive migration of $\tau(x)$ from the Loaded End (LE) towards the Free End (FE) for whatever value of L_{Rfi} and by increasing δ_{Li}.

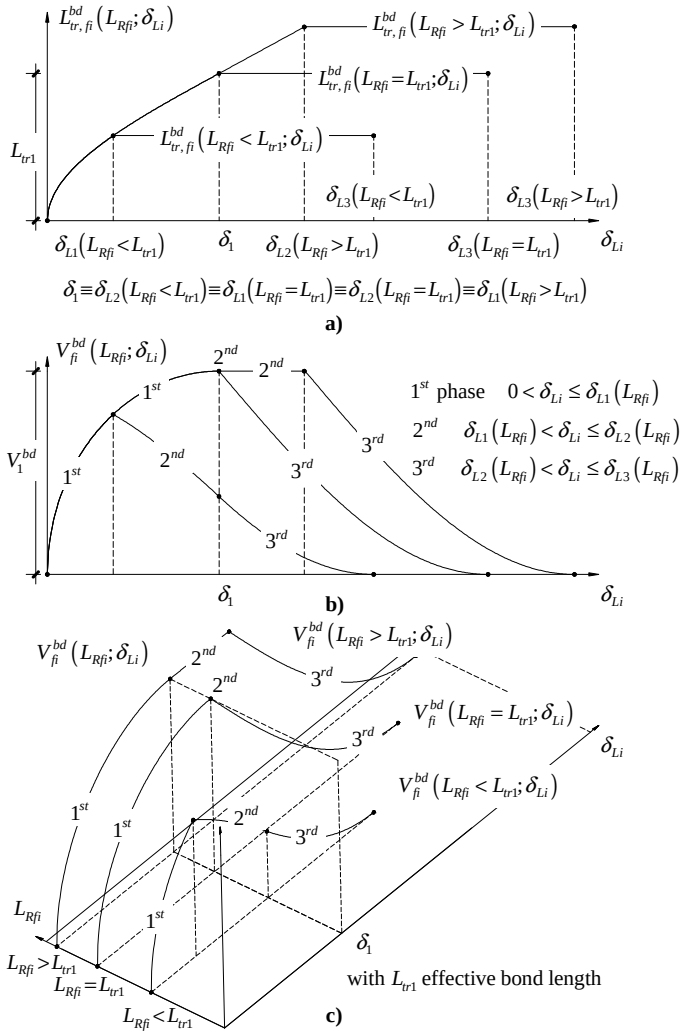

Fig. 4. Bond-based constitutive law of a single NSM FRP strip: (a) relationship between the bond transfer length $L^{bd}_{tr,fi}(\delta_{Li};L_{Rfi})$ and the imposed end slip δ_{Li} for different values of resisting bond length L_{Rfi}; (b) bi-dimensional and (c) three-dimensional representation of the relationship between the force transferrable by bond $V^{bd}_{fi}(\delta_{Li};L_{Rfi})$ and δ_{Li} for different values of L_{Rfi}.

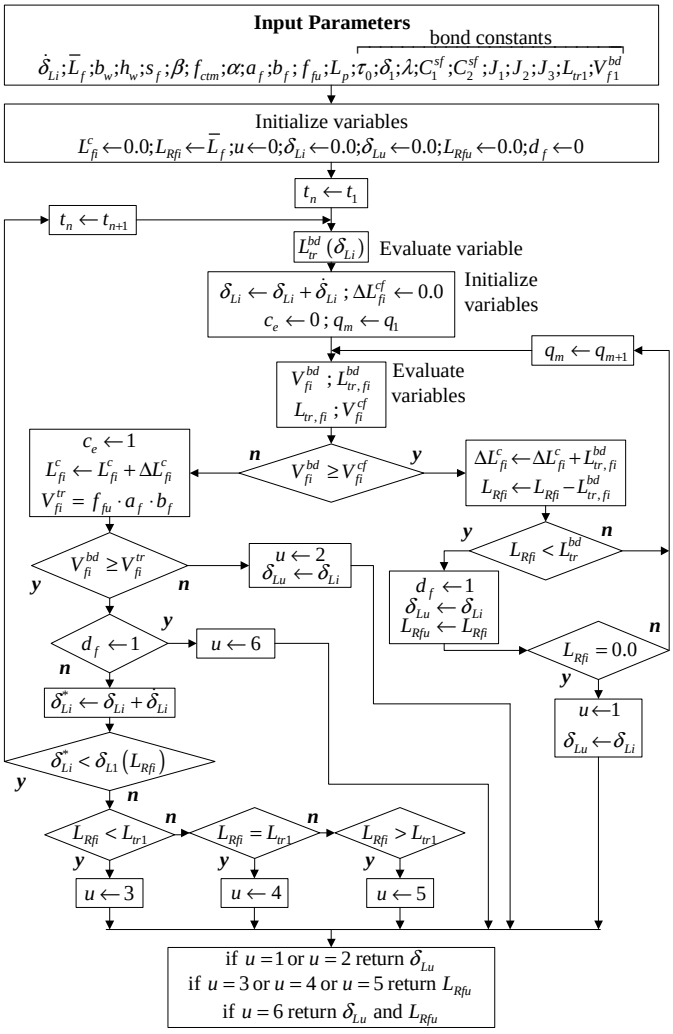

Fig. 5. Determination of the comprehensive constitutive law: flow chart.

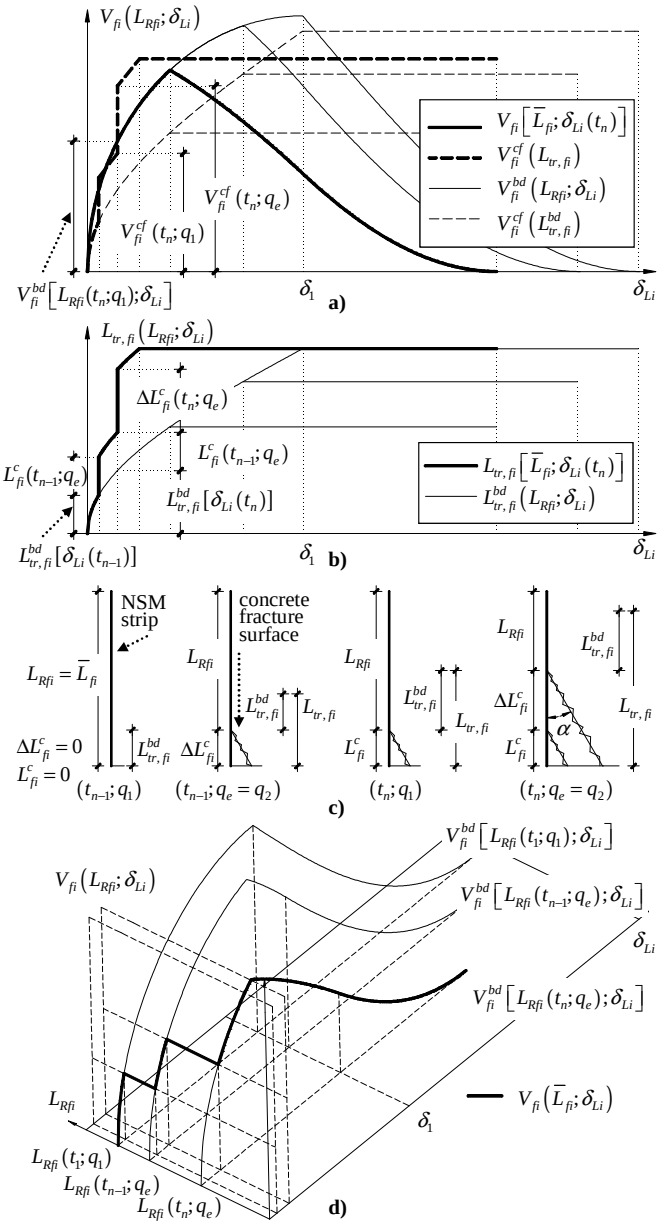

Fig. 6. Single NSM FRP strip comprehensive constitutive law in the case in which concrete fracture remains shallow: a) resulting constitutive law $V_{fi}\left(\bar{L}_{fi};\delta_{Li}\right)$ in a bi-dimensional representation, b) resulting overall transfer length $L_{tr,fi}\left(\bar{L}_{fi};\delta_{Li}\right)$, c) section of the concrete prism and occurrence of subsequent fractures and d) resulting constitutive law $V_{fi}\left(\bar{L}_{fi};\delta_{Li}\right)$ in a three-dimensional representation. Note that this plot has been done for an initial resisting bond length equal to the effective bond length but this does not affect the generality of the exposition.

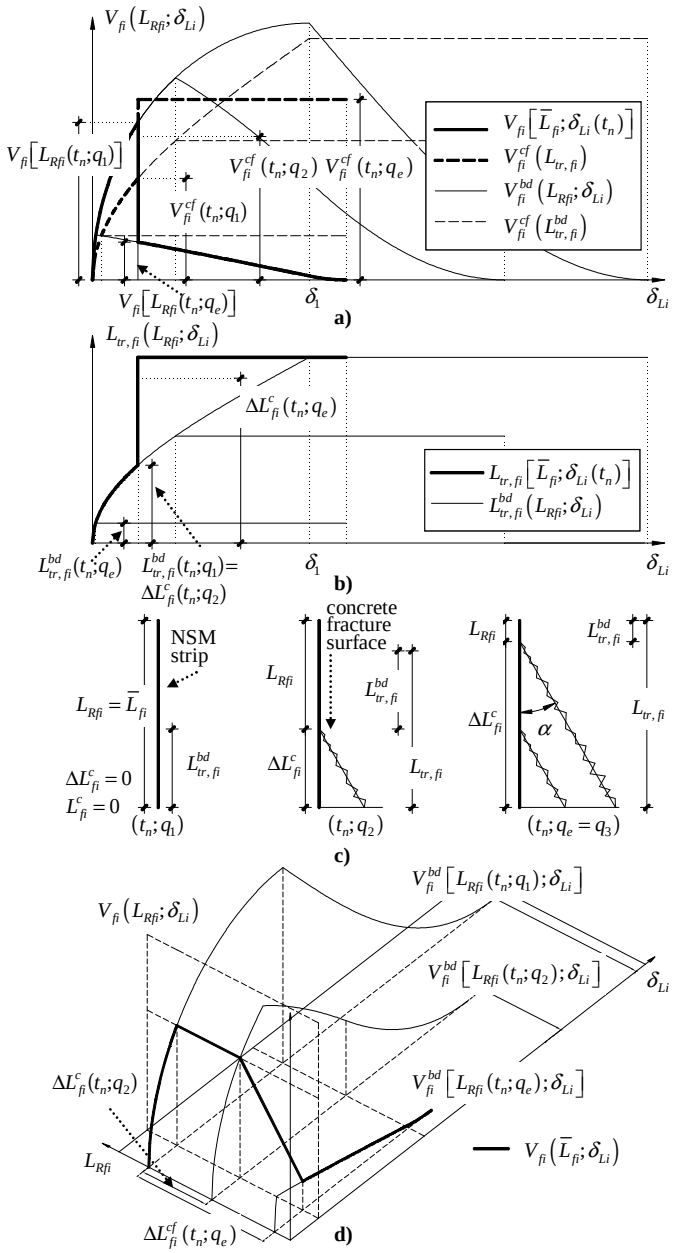

Fig. 7. Single NSM FRP strip comprehensive constitutive law in the case in which concrete fracture is deep: a) resulting constitutive law $V_{fi}\left(\overline{L}_{fi};\delta_{Li}\right)$ in a bi-dimensional representation, b) resulting overall transfer length $L_{tr,fi}\left(\overline{L}_{fi};\delta_{Li}\right)$, c) section of the concrete prism and occurrence of subsequent fractures and d) resulting constitutive law $V_{fi}\left(\overline{L}_{fi};\delta_{Li}\right)$ in a three-dimensional representation. Note that this plot has been done for an initial resisting bond length equal to the effective bond length but this does not affect the generality of the exposition.

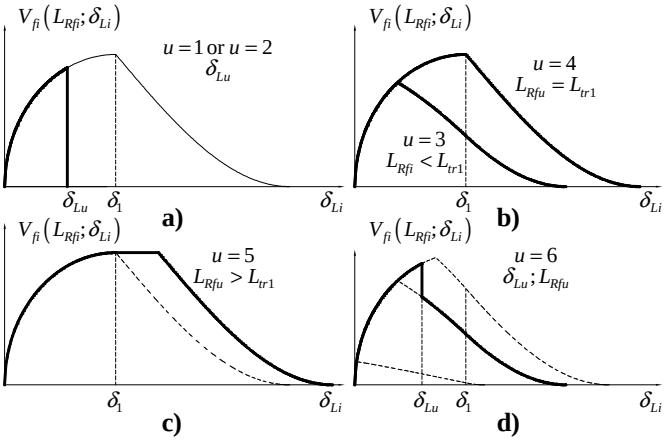

Fig. 8. Possible comprehensive constitutive law of a NSM FRP strip confined to a prism of concrete: (a) concrete that reaches the free extremity ($u=1$) or strip tensile rupture ($u=2$), superficial and/or absent concrete fracture and ultimate resisting bond length (b) smaller ($u=3$) or equal ($u=4$) or (c) larger ($u=5$) than the effective bond length and (d) deep concrete fracture ($u=6$).

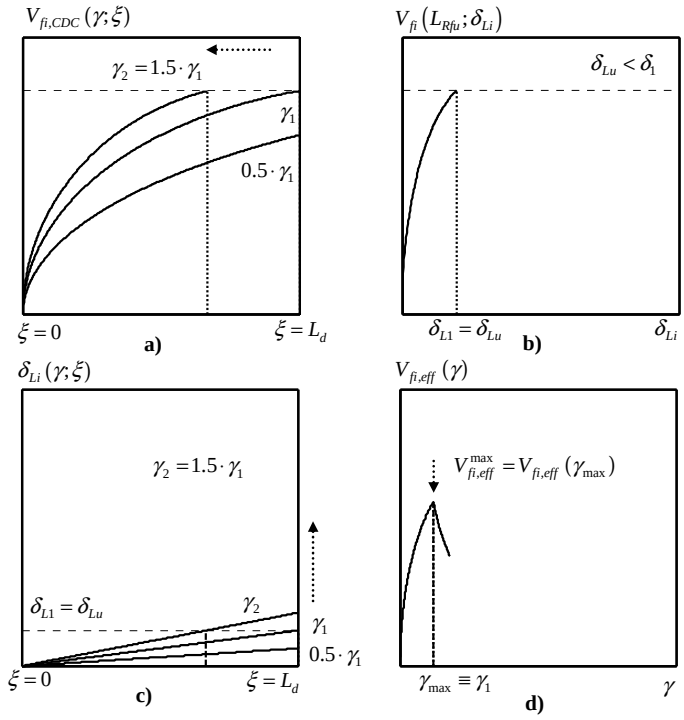

Fig. 9. Maximum effective capacity along the CDC for the cases of concrete fracture that reaches the strip's free extremity ($u = 1$) or strip's tensile rupture ($u = 2$): a) capacity $V_{fi,CDC}(\gamma;\xi)$ and c) imposed end slip $\delta_{Li,CDC}(\gamma;\xi)$ distribution along the CDC for different values of the CDC opening angle γ, b) comprehensive constitutive law and d) effective capacity as function of the CDC opening angle γ.

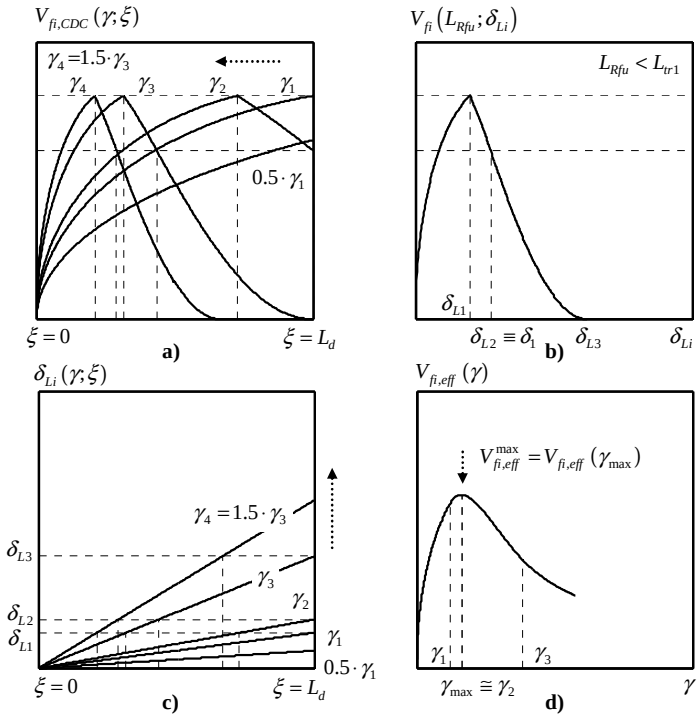

Fig. 10. Maximum effective capacity along the CDC for the case of shallow concrete fracture and an ultimate value of the resisting bond length smaller than the effective bond length ($u = 3$): a) capacity $V_{fi,CDC}(\gamma;\xi)$ and c) imposed end slip $\delta_{Li,CDC}(\gamma;\xi)$ distribution along the CDC for different values of the CDC opening angle γ, b) comprehensive constitutive law and d) effective capacity as function of the CDC opening angle γ.

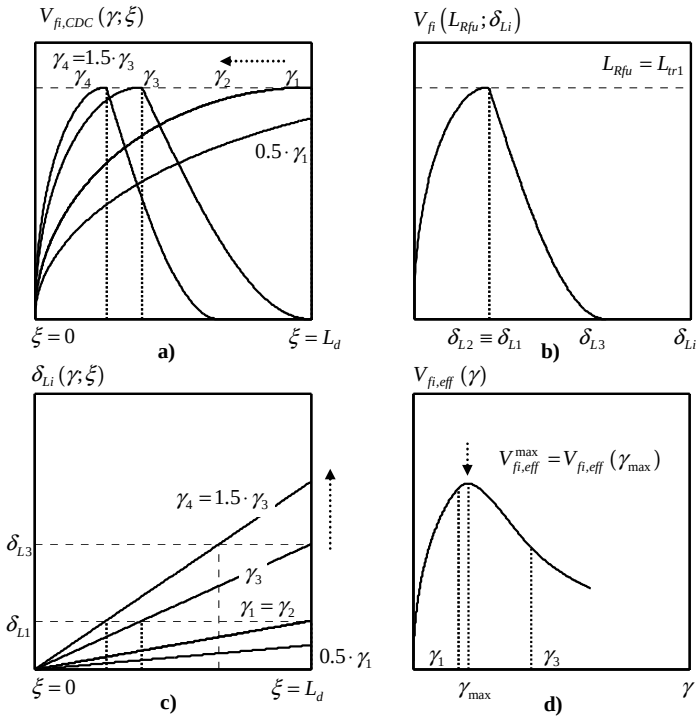

Fig. 11. Maximum effective capacity along the CDC for the case of shallow concrete fracture and an ultimate value of the resisting bond length equal to the effective bond length ($u = 4$): a) capacity $V_{fi,CDC}(\gamma;\xi)$ and c) imposed end slip $\delta_{Li,CDC}(\gamma;\xi)$ distribution along the CDC for different values of the CDC opening angle γ, b) comprehensive constitutive law and d) effective capacity as function of the CDC opening angle γ.

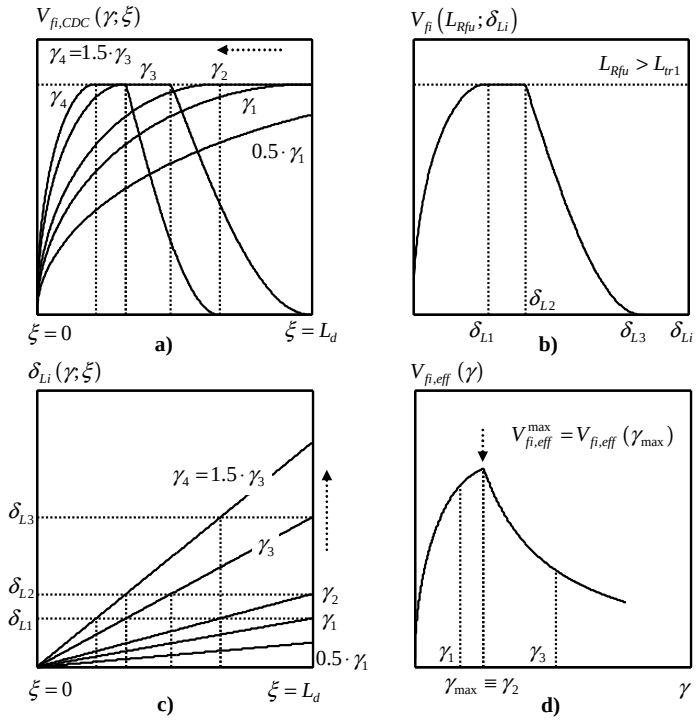

Fig. 12. Maximum effective capacity along the CDC for the case of shallow concrete fracture and an ultimate value of the resisting bond length larger than the effective bond length ($u = 5$): a) capacity $V_{fi,CDC}(\gamma;\xi)$ and c) imposed end slip $\delta_{Li,CDC}(\gamma;\xi)$ distribution along the CDC for different values of the CDC opening angle γ, b) comprehensive constitutive law and d) effective capacity as function of the CDC opening angle γ.

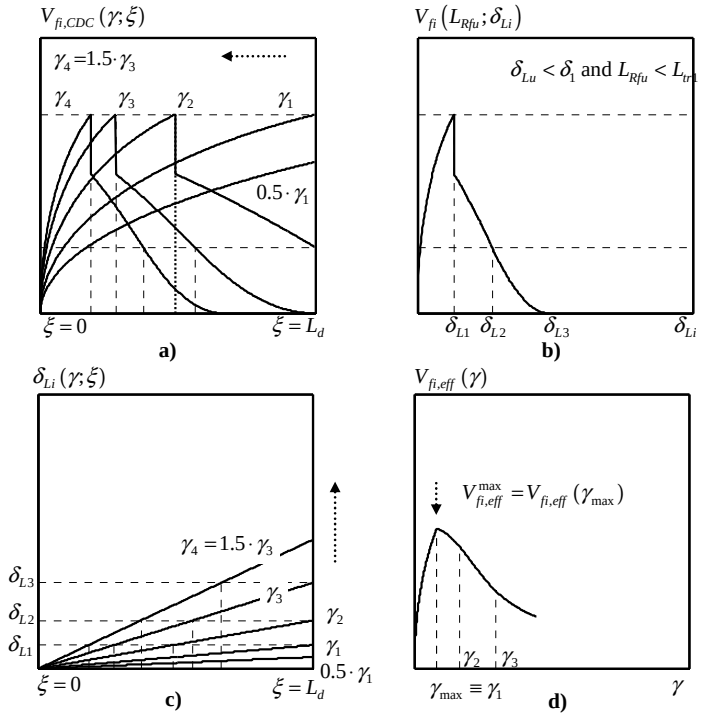

Fig. 13. Maximum effective capacity along the CDC for the case of deep concrete fracture ($u = 6$): a) capacity $V_{fi,CDC}(\gamma;\xi)$ and c) imposed end slip $\delta_{Li,CDC}(\gamma;\xi)$ distribution along the CDC for different values of the CDC opening angle γ, b) comprehensive constitutive law and d) effective capacity as function of the CDC opening angle γ.